



Calhoun: The NPS Institutional Archive
DSpace Repository

Theses and Dissertations

1. Thesis and Dissertation Collection, all items

1990-12

Stellar spectral line synthesis from an individual photon-following simulation

DeVogel, Gregory F.

Monterey, California: Naval Postgraduate School

<http://hdl.handle.net/10945/27571>

This publication is a work of the U.S. Government as defined in Title 17, United States Code, Section 101. Copyright protection is not available for this work in the United States.

Downloaded from NPS Archive: Calhoun



Calhoun is the Naval Postgraduate School's public access digital repository for research materials and institutional publications created by the NPS community. Calhoun is named for Professor of Mathematics Guy K. Calhoun, NPS's first appointed -- and published -- scholarly author.

Dudley Knox Library / Naval Postgraduate School
411 Dyer Road / 1 University Circle
Monterey, California USA 93943

<http://www.nps.edu/library>

AD-A242 970
■■■■■■■■■■

NAVAL POSTGRADUATE SCHOOL
Monterey, California



DA
C
J

THESIS

STELLAR SPECTRAL LINE SYNTHESIS
FROM AN
INDIVIDUAL PHOTON-FOLLOWING SIMULATION

by

Gregory Francis DeVogel

December 1990

Thesis Advisor:

Wm. Bruce Weaver

Approved for public release; distribution is unlimited.

91-17017
■■■■■■■■■■

91 12 4 011

UNCLASSIFIED

SECURITY CLASSIFICATION OF THIS PAGE

REPORT DOCUMENTATION PAGE				Form Approved OMB No. 0704-0188	
1a REPORT SECURITY CLASSIFICATION UNCLASSIFIED			1b RESTRICTIVE MARKINGS		
2a SECURITY CLASSIFICATION AUTHORITY			3. DISTRIBUTION / AVAILABILITY OF REPORT Approved for public release distribution is unlimited		
2b DECLASSIFICATION / DOWNGRADING SCHEDULE			5. MONITORING ORGANIZATION REPORT NUMBER(S)		
4. PERFORMING ORGANIZATION REPORT NUMBER(S)					
6a NAME OF PERFORMING ORGANIZATION Naval Postgraduate School		6b OFFICE SYMBOL (If applicable) PH	7a. NAME OF MONITORING ORGANIZATION Naval Postgraduate School		
6c. ADDRESS (City, State, and ZIP Code) Monterey Ca. 93943-5000			7b. ADDRESS (City, State, and ZIP Code) Monterey Ca. 93943-5000		
8a NAME OF FUNDING / SPONSORING ORGANIZATION		8b. OFFICE SYMBOL (If applicable)	9 PROCUREMENT INSTRUMENT IDENTIFICATION NUMBER		
8c. ADDRESS (City, State, and ZIP Code)			10 SOURCE OF FUNDING NUMBERS		
			PROGRAM ELEMENT NO	PROJECT NO	TASK NO
			WORK UNIT ACCESSION NO.		
11 TITLE (Include Security Classification) Stellar Spectral line synthesis from an Individual Photon following simulation					
12 PERSONAL AUTHOR(S) DeVogel Gregory F.					
13a TYPE OF REPORT Master Thesis		13b TIME COVERED FROM _____ TO _____		14 DATE OF REPORT (Year, Month, Day) December 1990	
15 PAGE COUNT 65					
16 SUPPLEMENTARY NOTATION The views expressed in this thesis are those of the author and do not reflect the official policy or position of the department of Defense or the U. S. Government					
17 COSATI CODES			18 SUBJECT TERMS (Continue on reverse if necessary and identify by block number)		
FIELD	GROUP	SUB-GROUP	Simulation, Solar absorption lines, Radiative transfer theory		
19 ABSTRACT (Continue on reverse if necessary and identify by block number) A stochastic stellar atmosphere model which simulates the behavior of photons in the atmospheres of stars by following individual photons is described and tested. The model accounts for stellar turbulence, atmospheric curvature, stellar rotation, collisional excitation, collisional de-excitation, and stellar winds. Testing shows that this new method of stellar radiative transfer is successful in simulating all of these processes. Particular results of interest include simulation of solar limb darkening and spectral synthesis of three different solar absorption lines; Ti $\lambda 6258.1 \text{ \AA}$, K $\lambda 4044.1 \text{ \AA}$, and Sr $\lambda 4607.3 \text{ \AA}$.					
20 DISTRIBUTION / AVAILABILITY OF ABSTRACT <input checked="" type="checkbox"/> UNCLASSIFIED/UNLIMITED <input type="checkbox"/> SAME AS RPT <input type="checkbox"/> DTIC USERS			21 ABSTRACT SECURITY CLASSIFICATION UNCLASSIFIED		
22a NAME OF RESPONSIBLE INDIVIDUAL Dave Cleary			22b TELEPHONE (Include Area Code) 408 646-2828		22c OFFICE SYMBOL PH/C1

DD FORM 1473, JUN 86

Previous editions are obsolete.

SECURITY CLASSIFICATION OF THIS PAGE

S/N 0102-LF-014-6603

UNCLASSIFIED

Approved for public release: distribution is unlimited.

**STELLAR SPECTRAL LINE SYNTHESIS
FROM AN
INDIVIDUAL PHOTON-FOLLOWING SIMULATION**

by

Gregory F. DeVogel

Lieutenant, United States Navy

B. S., University of Washington, 1985

Submitted in partial fulfillment of the
requirements for the degree of

MASTER OF SCIENCE IN PHYSICS

from the

NAVAL POSTGRADUATE SCHOOL

December 1990


Author:


Gregory F. DeVogel

Approved by:


Wm. Bruce Weaver, Thesis Advisor


David D. Cleary, Second Reader


Karlheinz E. Woehler, Chairman,
Department of Physics

ABSTRACT

A stochastic stellar atmosphere model which simulates the behavior of photons in the atmospheres of stars by following individual photons is described and tested. The model accounts for stellar turbulence, atmospheric curvature, stellar rotation, collisional excitation, collisional de-excitation, and stellar winds. Testing shows that this new method of stellar radiative transfer is successful in simulating all of these processes. Particular results of interest include simulation of solar limb darkening and spectral synthesis of three different solar absorption lines; Ti $\lambda 6258.1 \text{ \AA}$, K $\lambda 4044.1 \text{ \AA}$, and Sr $\lambda 4607.3 \text{ \AA}$.

A-1

Table of Contents

I.	INTRODUCTION	1
A.	BACKGROUND ON RADIATION TRANSFER	2
1.	NLTE	5
2.	Winds	5
B.	CURRENT STELLAR ATMOSPHERE MODELING	5
1.	Continuum	6
2.	Line modeling	7
3.	Spectral synthesis	9
4.	Limitations	11
5.	Other approaches	12
C.	STOCHASTIC PHOTON-FOLLOWING SIMULATION	14
1.	Motivation for SAM	14
2.	SAM1_13	16
3.	Shortcomings of SAM1_13	21
II.	OBJECTIVES OF THIS THESIS	22
III.	IMPROVEMENTS TO SIMULATION	23
A.	STELLAR ROTATION	23
B.	COLLISIONAL EXCITATION AND DE-EXCITATION	26
C.	INTERPOLATION TABLES	30
D.	OPTIMIZATION OF PHOTON STARTING DEPTH	30
E.	REDISTRIBUTION	31
IV.	TESTING AND RESULTS	36

A. MEAN FREE PATH	36
B. COMPARISON TO OBSERVATION	39
1. Convergence	39
2. Line synthesis	41
C. LIMB DARKENING	46
D. STELLAR TURBULENCE	48
E. STELLAR WINDS	49
V. CONCLUSIONS	52
APPENDIX A. SOLAR ATMOSPHERIC PARAMETERS	53
LIST OF REFERENCES	56
INITIAL DISTRIBUTION LIST	58

ACKNOWLEDGEMENT

This work would not have been possible without the advice, direction, and support of Dr. Bruce Weaver. I sincerely appreciate the time and effort contributed by Dr. Weaver to this thesis. With his busy schedule, I am not sure how or where he found the time. In addition, I would like to thank Dave Gillingham and Dr. Ana Torres-Dodgen for their insight and help.

Finally, I would very much like to thank my fiancée, who gave me the strength and support to complete this work. It is a miracle she is still willing to marry me!

I. INTRODUCTION

Recent advances in spectroscopy have led to a heightened interest in radiative transfer theory. As R. P. Kudritzki stated (Ref. 1)

If one looks at all the published papers resulting from extremely expensive space experiments or extensive ground based observations using large telescopes then a disturbingly large fraction contain simply line identifications, radial velocities, and only qualitative arguments. In view of all the financial and engineering effort that goes into the development of our modern instruments this is, of course, not enough.

What is lacking is a comprehensive, workable, quantitative, radiative transfer theory with which to extract as much information as possible from available stellar spectra. The principle problem faced by modern radiative transfer theory is the treatment of non-local thermodynamic equilibrium (NLTE) portions of stellar atmospheres. A few examples are: B- and A-type supergiant stars where NLTE theory is needed in the photosphere and the wind region, solar-type stars where strong absorption lines occur in the upper photosphere and the chromosphere; pre-main sequence stars with high mass loss and disks that protrude into the photosphere; and, probably the most complex case, O-type stars, where all LTE assumptions breakdown completely even deep in the photosphere.

Many different theoretical techniques have been applied to the problem of radiative transfer with varying degrees of success. In this paper, a new approach which follows individual photons through the stellar atmosphere of the star is examined.

A. BACKGROUND ON RADIATIVE TRANSFER THEORY

Radiative transfer theory is the study of how photons propagate through a medium. The theory has its origins in astronomy and the study of star atmospheres and spectra. But there are many additional military and civilian applications of radiative transfer theory (i.e., fusion bomb triggering, nuclear radiation transfer, atmospheric sciences).

To describe the interaction of matter and light it is necessary to characterize the state of the matter as well as that of the radiation field. Typically, the assumption of thermodynamic equilibrium (TE) or local thermodynamic equilibrium (LTE) is made to simplify this characterization. These assumptions significantly reduce the complexity of many of the radiative transfer computations. A quick review of these assumptions is in order. TE is the most restrictive case. A gas in TE will satisfy the following conditions:

1. Each species of gas particle will have a Maxwellian velocity distribution specified only by its mass and a temperature;
2. The distribution of the excited states of each ion will be accurately described by Boltzman's law specified only by the energies of excitation and a temperature;
3. The distribution of the ionized states of the atoms is accurately described by Saha's equation, again specified only by the energies of ionization and a temperature; and
4. Radiation intensity is accurately described by Planck's function specified only by a temperature.

It is important to note that in TE, the same temperature variable is utilized in all four relationships given above.

TE can only be achieved in an isolated system, so that the gas can not interchange any energy or mass with its surroundings. It is obvious that this condition is rather stringent and difficult to meet in a stellar atmosphere.

Since true TE cannot be fully justified, the less stringent LTE is usually invoked. In this second case, the gas will have TE characteristics over a local temperature zone. This assumption is justified when collisions among atoms of the gas occur rapidly enough to be the dominate cause of excitation. When this occurs, the kinetic temperature of the atoms in the local region can be used to accurately describe the gases' atomic properties. The fourth assumption will not hold for the LTE case because radiation escaping from deeper regions of the star cannot be described by the kinetic temperature of the local region; therefore, the radiation field can deviate arbitrarily from the Planck distribution.

The LTE assumption is a good description of the state of the matter deep in the photosphere of a star, where the majority of the energy is transferred via conduction or convection. This is for two reasons: 1) due to the high opacity, little radiation (energy) can escape directly, thus preserving energy conservation; and, 2) use of Boltzman's equation is justified because collisions are the main mechanism for atomic excitation thus allowing the excitation to be described by a single temperature. The LTE assumption begins to break down as the collisional transition rates of the ions approach the radiative transition rates. This decrease in collisional rates relative to the radiative rates occurs as the photons work their way up through the atmosphere during which the density of the gas and the kinetic temperature of the atoms decreases as energy is radiated away.

When the LTE assumption is no longer valid, the state of the gas can be calculated by statistical equilibrium (SE) methods. This approach balances the number of transitions *due to all processes* into and out of a given atomic level. This method is very difficult given the large number of energy levels and ionization states available to an atom. The method of statistical equilibrium is always valid

and the assumptions of LTE and TE are only special cases of SE.

With an understanding of the characterization of the medium, the radiative transfer equation is

$$\frac{dI_{\nu}}{d\tau_{\nu}} = I_{\nu} - S_{\nu} \quad (1)$$

where: I_{ν} = initial intensity as a function of frequency,

S_{ν} = source function as a function of frequency, and

τ_{ν} = optical depth as a function of frequency.

τ_{ν} and S_{ν} are given by

$$\tau_{\nu} = \int_0^L \kappa_{\nu} \rho dx, \text{ and} \quad (2)$$

$$S_{\nu} = \frac{j_{\nu}}{\kappa_{\nu}} \quad (3)$$

where: dx = geometrical depth,

L = path length,

ρ = density,

κ_{ν} = extinction coefficient ($\frac{cm^2}{g}$), and

j_{ν} = emission coefficient ($\frac{ergs}{g \text{ rad}^2}$).

The simplicity of equation (1) is deceiving. The complexity of the radiative transfer problem lies in determining the properties of κ_{ν} and j_{ν} . κ_{ν} and j_{ν} are dependent on the intensity which renders equation (1) a first order non-linear differential equation vastly complicating the problem.

Radiative transfer theory has been successful in explaining many features of stellar spectra. There are some important problems in which the restrictive assumptions of this theory fail to adequately describe the stellar atmosphere.

1. NLTE

Some of the more important spectral lines (i.e., strong absorption lines due to H, He, and metals) have non-LTE (NLTE) characteristics. This is because the line centers are formed high in the atmosphere where the density and kinetic temperature are low and radiative processes dominate over collisional processes. This NLTE behavior is not restricted to exotic high-temperature, high-luminosity stars; the sun contains several NLTE lines of interest. The importance of understanding NLTE line formation can not be over emphasized. Spectral measurements of faint stars typically can only detect strong absorption lines over background noise. Many of these absorption lines are NLTE in nature. Therefore an understanding of this NLTE line formation region is of paramount concern.

2. Winds

Radiatively driven winds in stellar atmospheres are an additional problem for the LTE assumptions. Many stars, particularly high-temperature, high-luminosity, very young, and very old stars, have rapid mass loss (typically 1 earth mass/yr) via radiatively-driven winds. These winds produce expanding stellar atmospheres where the LTE assumptions quickly break down. These expanding atmospheres also preferentially Doppler shift line profiles, which complicates the radiative transfer problem. Loss of matter must also be considered when analyzing the validity of the LTE assumption. Boltzman's equation requires a closed system in which the total mass of the system is conserved. Rapid mass loss is in violation of this requirement.

B. CURRENT STELLAR ATMOSPHERE MODELING

Stellar atmosphere modeling is an attempt to reconstruct the structure of the stellar atmosphere based on spectral observations and physical laws. The complexities of the dynamics of the atmosphere as well as the complexities of radiative

transfer theory prohibit direct measurement of many of the physical parameters. Therefore, a model is hypothesized to generate the observed spectral information. Once the model has been constructed which reproduces the observed information, additional observations can be made to further test the model. While this may not produce unique atmospheric parameters, stellar atmosphere modeling has become an indispensable tool in the analysis of stellar spectra. Most models contain the following simplifications:

1. LTE is assumed throughout the atmosphere;
2. Plane-parallel geometry is assumed ignoring atmospheric curvature;
3. Hydrostatic equilibrium is assumed neglecting any mass losses;
4. Fine structure is negligible (i.e., granulations, flares, sunspots); and
5. Magnetic fields are excluded.

Stellar modeling can be divided into three distinct types: continuum, line, and spectral synthesis. Each method will be examined further in the next three sections.

1. Continuum modeling

Continuum modeling seeks to reproduce the characteristics of a stars continuum radiation. The source function is calculated from the Planck distribution at a given depth of formation. This quantity is referred to as the surface flux. The extinction term from the radiative transfer equation (eq 1) is based on continuum absorption coefficient calculations and laboratory measurements of atomic properties (i.e., H , H^- , electron scattering). The standard radiative transfer integral is then solved, producing the calculated spectrum. The success of these types of models is remarkable considering their simplistic assumptions. Figure 1 shows a fit according to Melbourne [Ref. 2].

Continuum model comparison to Observations

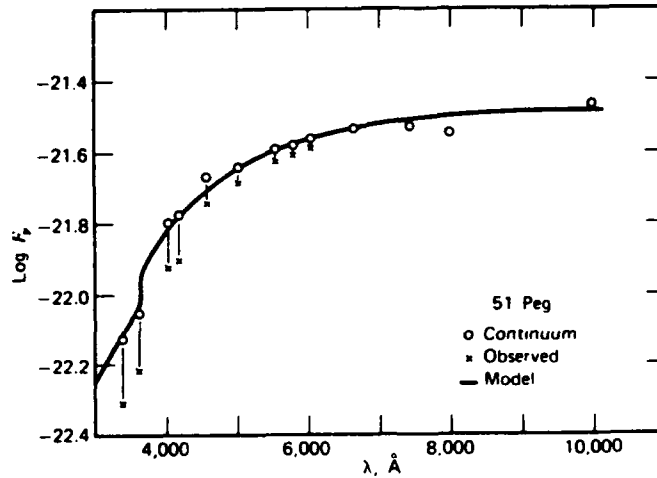


Figure 1: The observed energy distribution in 51 Peg(G5V) corrected for line absorption compared with model calculations [Ref. 2].

Note that the observed data has been adjusted to account for line absorption at the shorter wavelengths.

The continuum modeling technique contains three major problem areas: 1) absolute continuum flux calibration (i.e., where is the continuum located), 2) NLTE effects on the temperature gradient, and 3) interstellar reddening. The first two of these problems is intrinsic to the continuum modeling technique and not easily solved; interstellar reddening complicates comparisons to observed continuum.

2. Line modeling

Line modeling efforts have been directed at determining the shape of line absorption profiles. With accurate profiles much can be learned about stellar atmospheres. The line absorption profile is dependent on many important atmospheric

parameters (i.e., pressure, temperature, radiation field, rotation, winds, turbulence, depth of line formation, etc.). It is the interaction of these parameters that produces the absorption profile and thus reveals information about the conditions at formation of the line. In addition, line modeling provides information about the processes that produce various line profiles.

The radiative transfer equation (eq 1) is the basis of these calculations. But the central problem remains how to obtain an accurate source function. Typically, S_ν is approximated by a combination of a line-source function and a continuum-source function. The line-source function is calculated from LTE considerations and the continuum-source function is calculated from surface flux calculations. These calculations have produced good results when compared to actual absorption-line profiles. Figure 2 and 3 show the results of line modeling done by Carbon and Gingerich [Ref. 3], and Curtis and Jefferies [Ref. 4] respectively.

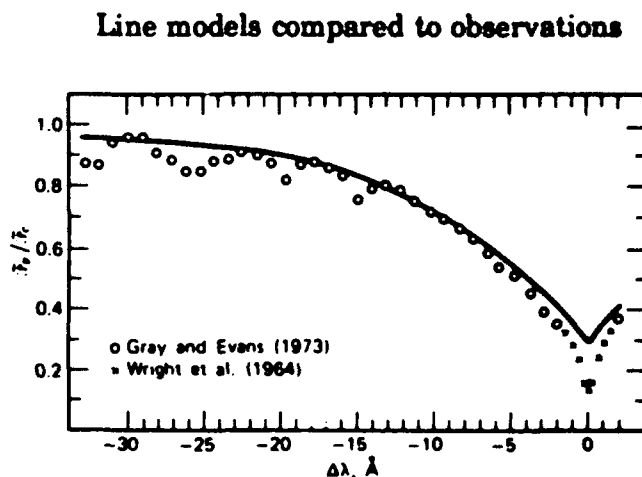


Figure 2: The observed H_γ profile in θ Leo compared with LTE line profile calculations. The model calculations fail to correctly model the line cores [Ref. 3].

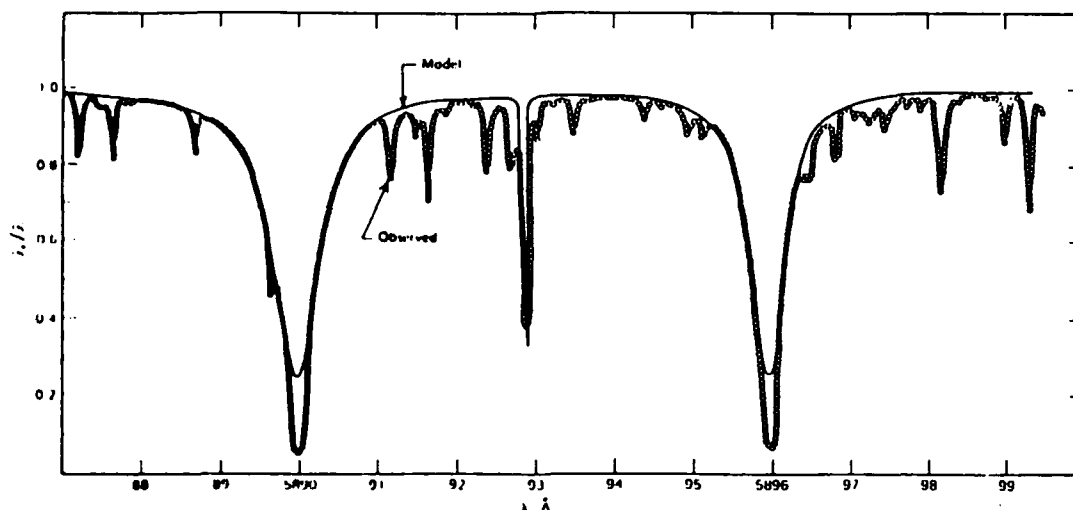


Figure 3: The observed Na D line profile compared with LTE line profile calculations. Again the model calculations fail to correctly model the line cores [Ref. 4].

The depths of the observed profiles are deeper than those calculated by line-modeling theory. This is one of the inadequacies of the current line-modeling theory. Gray cites the effects of turbulence and NLTE population levels as typically deepening line cores [Ref. 5]. Inclusion of these phenomena improves line fits markedly but some differences still remain. The line-modeling-technique limitations are not only confined to NLTE effects at line cores. Weak-line calculations also fail to match theoretical curves of growth. Curves of growth describe the theoretical growth of an absorption line as a function of abundance, temperature, and pressure. Weak-line calculations fail to match these curves although inclusion of turbulence improves the fits.

3. Spectral synthesis

Spectral synthesis is a method of spectral analysis developed to calculate the chemical abundance in stellar atmospheres. High-resolution observations of spectral lines are compared to the synthesized lines. The individual abundances

of the atoms are adjusted until a good fit in the synthesized line is achieved, thus determining the chemical composition of the star. The intensities of the spectral lines are calculated by evaluating the standard radiative equation (eq 1). The results of some spectral synthesis are shown in Figure 4 and 5.

Spectral synthesis compared with observations

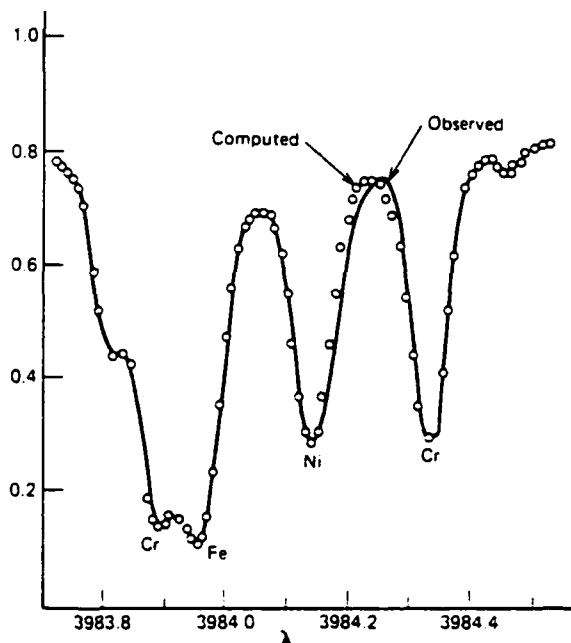


Figure 4: An observed portion of the solar spectrum compared with Ross and Aller spectral synthesis [Ref. 6].

Figure 4 is a comparison of computer synthesized lines to observed solar lines [Ref. 6]. The fit is fairly good, although turbulence effects have been added. Figure 5 is the synthesized spectrum of a carbon star (TX Psc) compared to observations [Ref. 7]. Although the fit shows significant deviation from observations, Figure 5 shows how even very crowded regions of the spectrum can be synthesized.

This third approach contains many of the same problems as the line-modeling method. The emphasis in this method has been on the problem of line

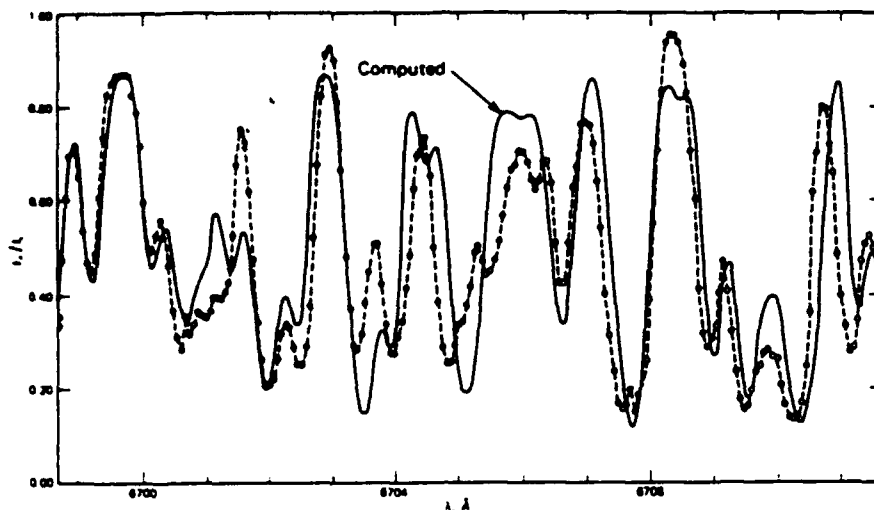


Figure 5: The observed spectrum of TX Psc compared with Synthesized spectrum [Ref. 7].

blending in crowded regions and not on the line profile itself.

4. Limitations

Although these modeling methods have been very successful, each does possess some limitations as noted. In addition, all of these methods contain four generic problems: 1) the assumption of a plane-parallel geometry, inappropriate for large extended stellar atmospheres; 2) they lack an easy method by which to incorporate stellar winds and rotation; 3) Line profiles and continuum models fail to reproduce this observed limb darkening behavior* across the solar disk; and 4) LTE atmospheres are assumed.

* Observations of the sun's disk reveal that intensity decreases as observations near the solar limb.

5. Other approaches

In an effort to solve the NLTE problem, Kudritzki [Ref. 8] used the method of linearization proposed by Auer and Mihalas [Ref. 9] to develop a computer code designed to model the structure of the NLTE atmosphere. The method accounts for all possible coupling between variables at all different depths within the constraints of statistical, hydrostatic, and radiative equilibrium. This is essentially the statistical equilibrium method. To show the complexities of these calculations, the O II Grotrian diagram used by Becker and Butler [Ref. 10, 11] is shown in Figure 6.

Grotrian diagram

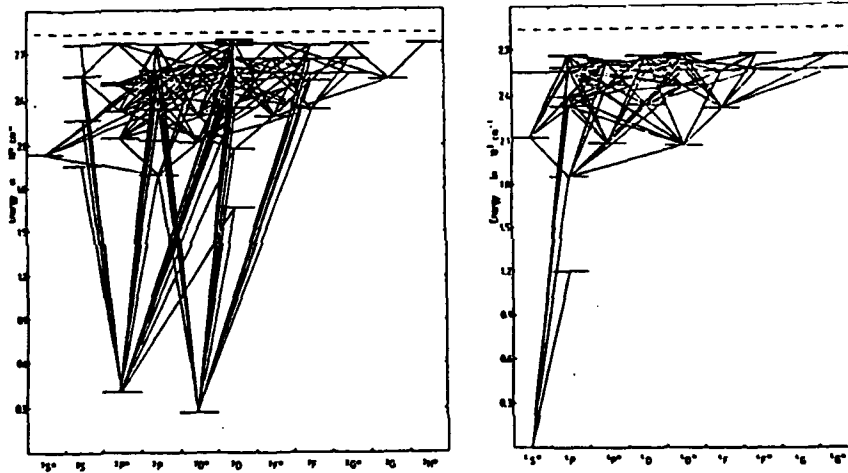


Figure 6: O II Grotrian diagram showing the 200 different transition which must be calculated [Ref. 10, 11].

The computer code must be given, or calculate, all atomic parameters and calculate all transition rates into and out of these 200 different atomic energy levels. Kudritzki [Ref. 12] has demonstrated that a large number of transitions are necessary for acceptable accuracy. With accurate atomic parameters, the results of this method can be highly accurate (Figure 7). Discrepancies in the line core were

corrected for by Herrero [Ref. 13] by including new collisional broadening terms and coupling between H and He II.

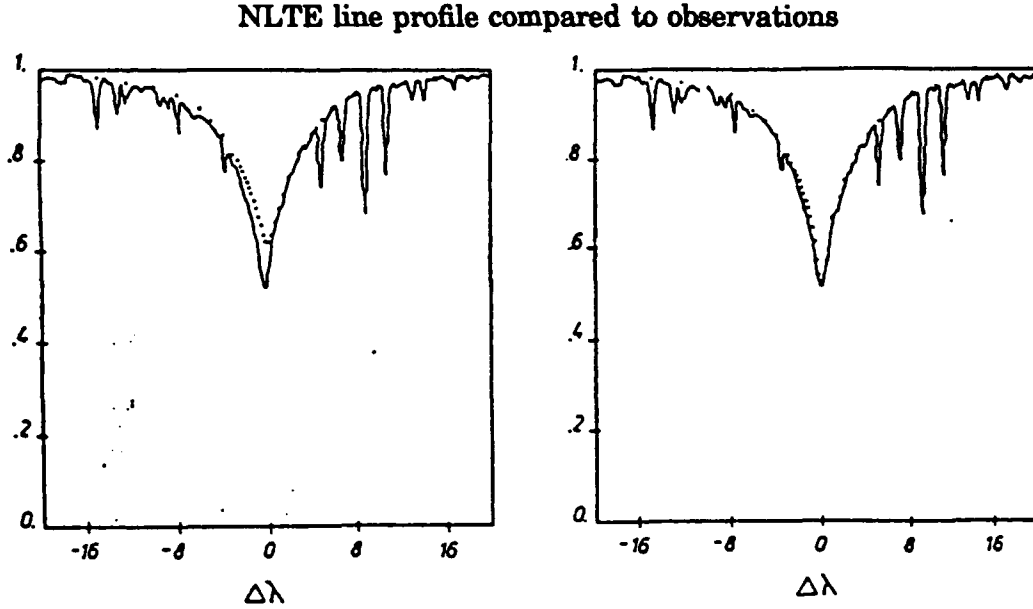


Figure 7: Observed H_γ profile of the O 9.5 V star τ Sco compared to NLTE calculations [Ref. 9] (left) and recent improvements by Herrero [Ref. 13] (right).

In an effort to explain multi-line wind transfer problems, Abbott and Lucy [Ref. 14] developed a Monte Carlo technique for the exploration of stellar wind effects on the spectra from stars with strong stellar winds. The atmospheric parameters used by Abbott and Lucy were from Kudritzki, Simon, and Hamann [Ref. 15]. Their technique follows energy packets, which may be as small as $h\nu$, from the top of the photosphere to their emergence through the stellar wind portion of the upper atmosphere. In this way wind effects can be simulated and wind-driving forces explored. Results of this technique are shown in Figure 8 and reveals general agreement with observations of ζ Pup in the ultraviolet.

Wind simulation compared to observations

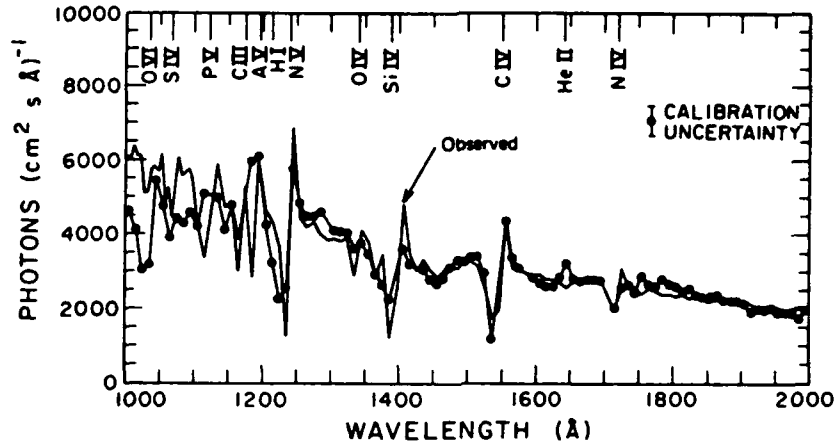


Figure 8: Abbott and Lucy fit to observed ζ Pup spectrum. Prominent features are identified on the top axis [Ref. 14].

C. STOCHASTIC PHOTON-FOLLOWING SIMULATION

1. Motivation for SAM

In view of the limitations with current atmospheric modeling and radiative transfer methods a new approach has been explored by W. B. Weaver at the Monterey Institute for Research in Astronomy. He has developed a stochastic Monte Carlo stellar atmosphere model (SAM). The advantages of this approach are listed below:

1. Interaction of photons and matter can be modeled explicitly and in detail permitting easy inclusion of NLTE effects;
2. Computations are done in spherical geometry;
3. Influence of stellar rotation is included;

4. Influence of stellar winds is included;
5. $2 \frac{1}{2}$ dimensional geometry is used naturally reproducing limb darkening; and
6. Output is in 2 dimensions; λ and θ ; where θ is the angle from the surface normal.

SAM is a true simulation, with the fundamental atomic processes being modeled. The advantage of this approach allows the modeler to investigate fundamental physical processes, leaving the radiative transfer computations to the computer.

The theoretical concept behind SAM is simple. At large optical depth, the radiation field is accurately described by the Planck function. Individual photons selected from the Planck distribution are followed as they migrate through the atmosphere. The properties of the photosphere are then accurately described by the LTE assumptions except, as stated before, for the radiation field. But by keeping track of the photons from the deeper region of the atmosphere, where the Planck function is valid, an accurate picture of the radiation field can be produced. In other words, SAM is able to reproduce both the radiation field as well as the state of the atoms in the important LTE region.

If one then continues into the NLTE region, the radiation field determined in LTE will help to formulate the characteristics of the NLTE portion of the atmosphere, thus approximating a solution to the NLTE radiation transfer problem.

Stellar wind effects can also be simulated. The outer atmosphere of SAM can easily be set in motion. This allows modelers to gain insight into the effects of rapidly moving atmospheres on line profiles.

2. SAM1_13

SAM1_13, the most recent version of SAM, is used as the starting point for this thesis. The method employed by SAM1_13 to simulate the radiative transfer problem is to generate a number (usually 500,000 photons/Å) of photons and distribute these photons evenly over the wavelengths in question. The assumption being the Planck function is flat over a few angstroms.

Photons are started at a calculated thermalization depth, usually deep within the photosphere. The calculations of thermalization depth are based on continuum photons with optical depth of 10. The individual photons are now permitted to migrate through the atmosphere. Random absorption probabilities are produced for continuum and line processes. Since continuous variation of atmospheric properties is impractical, atmospheric parameters are held constant for one to ten percent absorption probability. These small absorption probabilities are added until the initial randomly chosen absorption probability is reached. This procedure is followed for both line and continuum processes. The lengths traveled for the two processes are then compared, with the shortest being chosen by the computer as the absorption process the photon undergoes. At this point the photon is considered absorbed and a re-emitted photon is produced. For simplicity, collisional processes are not considered. The new photon is redistributed in wavelength and emission angle according to the absorption process involved (i.e., H^- absorption, line absorption). This process is continued for the photon until an assumed escape altitude is reached, usually the top of the photosphere, or it is destroyed by propagating back into the thermalization depth. Radiated photons are then collected into bins chosen by the user, typically of width .01 angstroms. Angle to the surface normal at the time of departure is also retained and radiated photons are binned accordingly.

SAM1_13 requires two programs to be run prior to actual photon generation. These programs read in atmospheric parameters and generate constants that

are needed by SAM. Figure 9 shows the order in which the different programs are run. Figure 10 shows the conceptual flow diagram of SAM's logic. Figure 11 is a detailed diagram of the photon absorption loops as described above.

SAM PROGRAM SEQUENCE

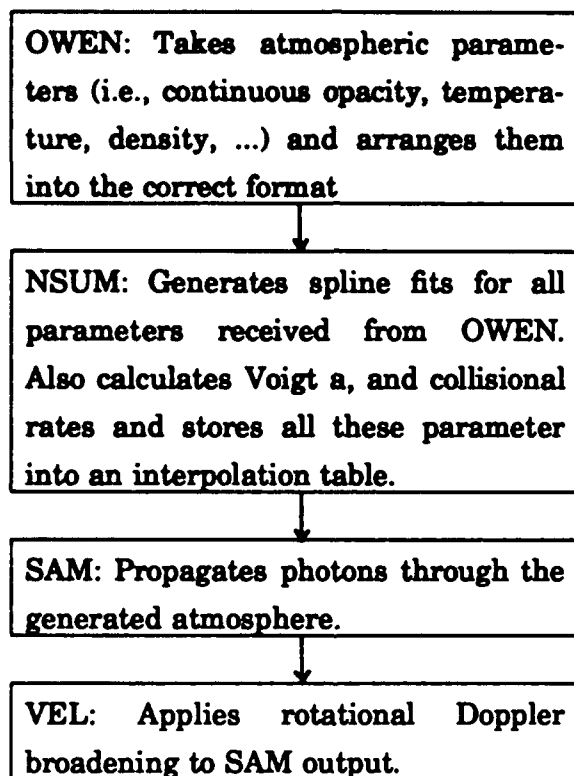


Figure 9: Order of execution of programs.

SAM CONCEPTUAL FLOW DIAGRAM

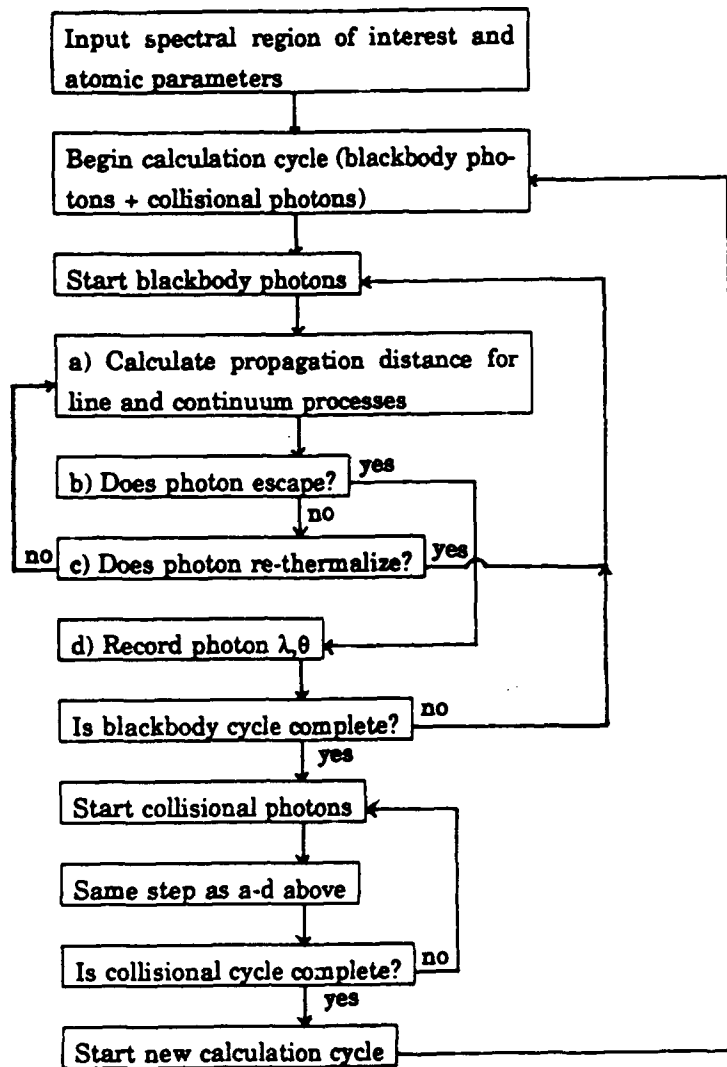


Figure 10: The logic flow of SAM during radiative transfer.

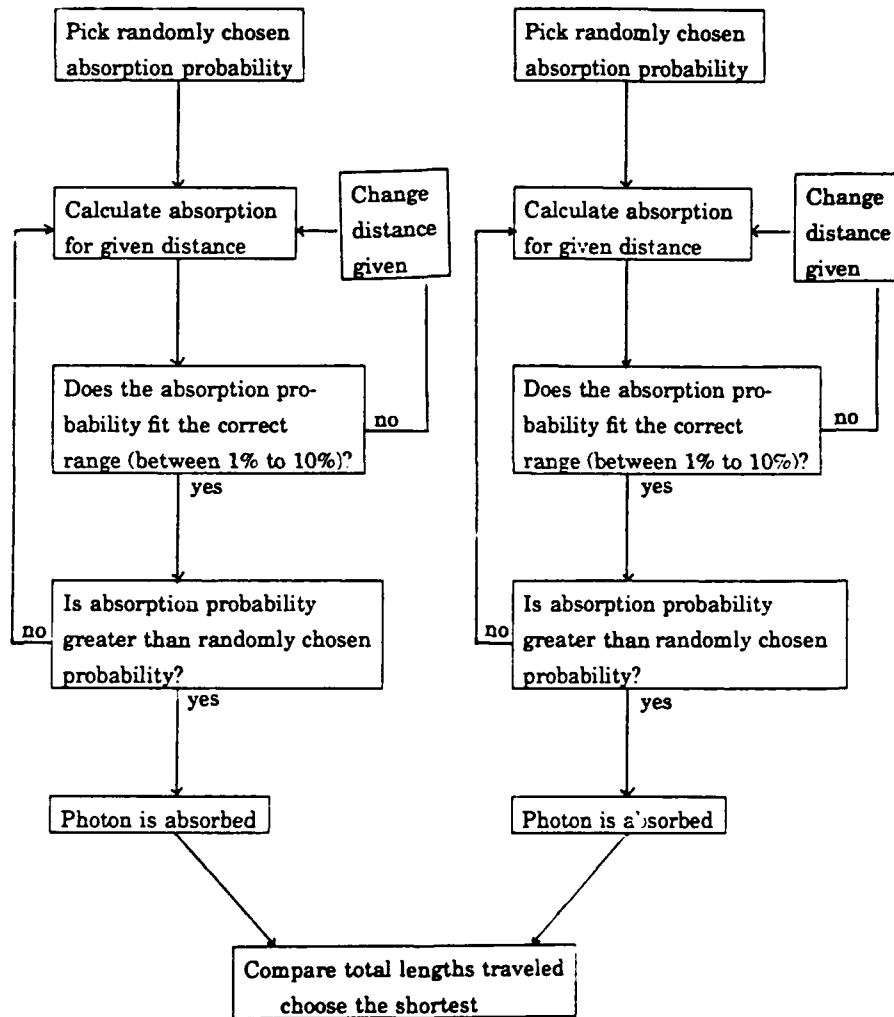


Figure 11: The logic flow of the two absorption loops in SAM.

Spherical geometry is the natural choice for photons propagating in SAM. The position of photon's can be described by the three spherical coordinates ρ , θ , and ϕ . Stellar atmospheres have spherical symmetry rendering ρ the only important coordinate in describing the photon's position. The photon's direction of propagation can be described by the two coordinates θ and ϕ . Where θ is the angle from the surface normal (ρ), and ϕ is the remaining angle defining the orientation of the plane formed by θ and ρ . The geometry is simplified by assuming that the orientation of this plane (ϕ angle) is symmetric for all photons. The ϕ dependence

can be condensed into the random θ calculations. With the condensation of ϕ , the coordinate system becomes a floating reference frame.

Geometry of SAM

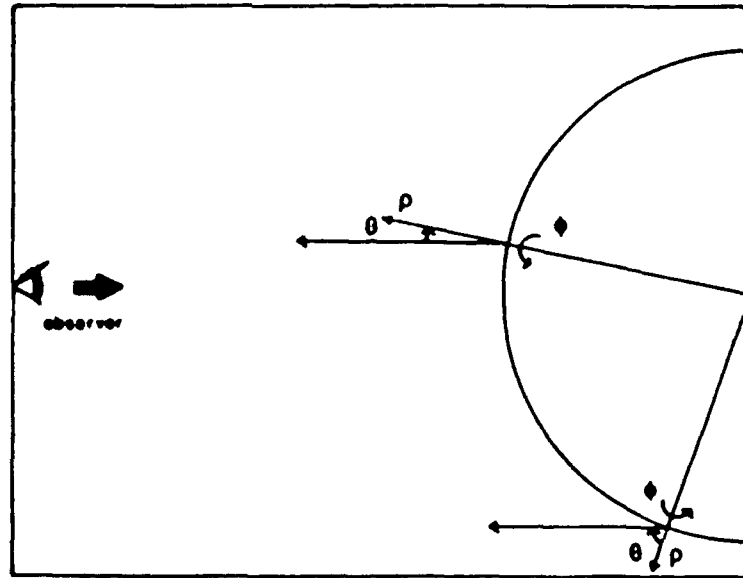


Figure 12: Orientation of ρ , θ , and ϕ .

In order to minimize computation time, all photons being radiated are assumed to propagate in the direction of the observer. At first, this may seem to be an inappropriate assumption, however, once the photons have left the atmosphere of the star, the θ dependence is removed and photons may be redistributed to propagate in the direction of the observer. Another way to look at this simplification is to think of the photons traveling backwards from the observer. When the photons are first absorbed at the upper surface of the star the incoming θ value is completely lost. It is at this point where θ can have any value, therefore a θ is chosen so the photon propagates in the direction of the observer.

3. The shortcomings of SAM1_13

Although SAM1_13 generates some interesting results, it has several shortcomings. 1) It fails to account for an unequal number of photons being produced and destroyed in the atmosphere above the thermalization depth by collisional processes. 2) It fails to account for energy conservation in the upper photosphere. This failure caused the upper atmosphere atoms to have LTE population levels when NLTE population levels would be more accurate. 3) It fails to have a mechanism for imposing stellar rotation effects onto the radiated photons. Rotation effects can be significant in some stars (i.e., line broadening of up to several angstroms). And 4) it contains simplified wavelength redistribution functions. In addition, it is felt that due to the large quantity of photons being generated and the many interactions each photon undergoes, a more rapid method of determining current atmospheric parameters is needed.

II. OBJECTIVES OF THIS THESIS

The main objective of this thesis is to improve SAM by including the following physical processes to provide a more complete model, including some NLTE effects. The physical processes being added are: stellar rotation, collisional excitation, collisional de-excitation, optimized photon starting depth, and an improved photon redistribution function. Additionally, minimizing the time required to calculate stellar atmosphere parameters will also be added. Once the improvements are made, SAM-generated lines are tested against three observed solar lines. These lines are Ti $\lambda 6258.1 \text{ \AA}$, $3d^3 4s - 3d^3 4p$, multiplet # 104, J 4-5; K $\lambda 4044.1 \text{ \AA}$, $4s-5p$, multiplet # 3, J $\frac{1}{2} - 1\frac{1}{2}$; Sr $\lambda 4607.3 \text{ \AA}$, $5s^2 - 5s 5p$, multiplet # 2, J 0-1. In addition, a comparison of the SAM-generated limb-darkening with the observed solar limb-darkening is made. Finally, an attempt is made to reproduce the characteristic structure observed in the spectra of stars with strong non-thermal winds. Although NLTE features are programmed into SAM (i.e., two temperatures for the outer photosphere), no attempt is made in this work to generate NLTE outer atmosphere atomic population levels.

III. IMPROVEMENTS TO SIMULATION

A. STELLAR ROTATION

Doppler shifting due to stellar rotation can significantly broaden observed line profiles. Since this is due to the integration of shifted, unbroadened lines from all portions of the disk visible to the observer, the total amount of light removed from the continuum is unchanged. At high rotational velocities, a few hundred kilometers per second, additional line broadening can be as much as several angstroms. Inclusion in SAM is necessary to correctly reproduce line profiles from stars rotating faster than 1 km/sec. The star is assumed to rotate as a solid body. This assumption is justified for many stars. For example the differential rotation for the sun from the equator to the 75° latitude is only 25%. Because SAM follows individual photons as they travel through the rotating stellar atmosphere, Doppler shifts within the atmosphere (internal Doppler shifts) must be examined as well as those affecting the observations of an external observer (external Doppler shifts).

There are no internal Doppler shifts because of the solid body assumption. Since two internal points in the atmosphere have no relative motion, no Doppler shifting can occur to a photon traveling between these two internal points.

The only broadening due to rotation comes from external Doppler shifts. Figure 13 shows photons escaping from the limbs of the star which will appear to the observer as blue and red shifted with respect to the center of the disk.

Each exiting photon in SAM must be Doppler shifted according to its exit location. The output of SAM is divided into angular increments. A rotating body inclined at an angle i to the line of sight of the observer can have its surface divided into a series of strips of unique radial velocities. Superimposed over the angular divisions of SAM are these unique radial velocity strips. In a separate software routine called VEL, the geometrical regions are calculated and the individual photons from each region are then Doppler shifted as appropriate. The

Photon Doppler shift diagram

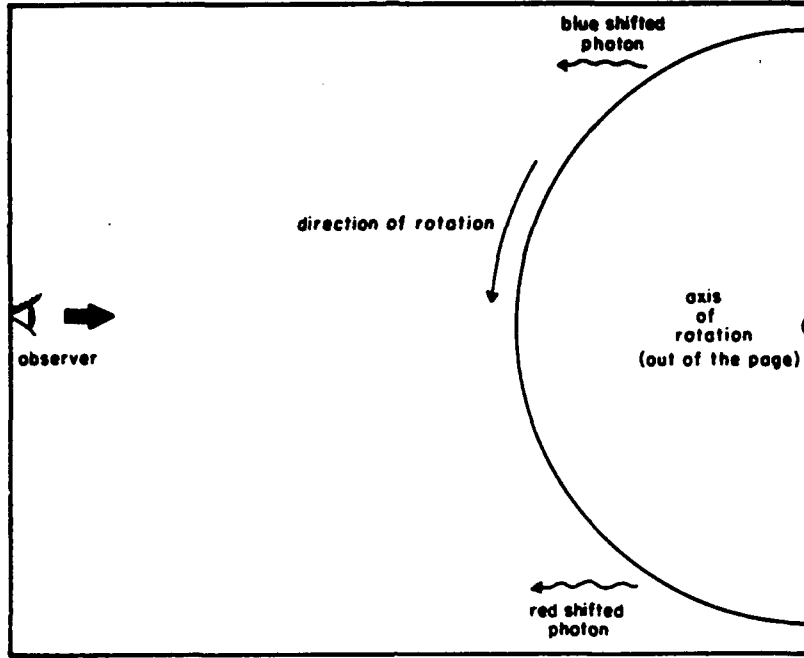


Figure 13: Photons are Doppler shifted as seen by the observer depending on the portion of the star from which they radiate.

general equation for this procedure is

$$NP(v,r) = \sum_{v=v_i}^{v_f} \sum_{r=r_i}^{r_f} \sum_{v=v_i}^{v_f} A_p(v,r) NP(v,r) \frac{\lambda}{1+v_{rel}(v)} , \quad (4)$$

where $NP(v,r)$ = number of photons as a function of v and r ,

A_p = ratio of total area to partial area of rings and velocity strips, and

v_{rel} = ratio of strip velocity to speed of light.

The input rotational speed for VEL is equal to $v \sin(i)$. Figure 14 shows the geometric regions of interest and the complicated areas that must be calculated.

Velocity and angular regions

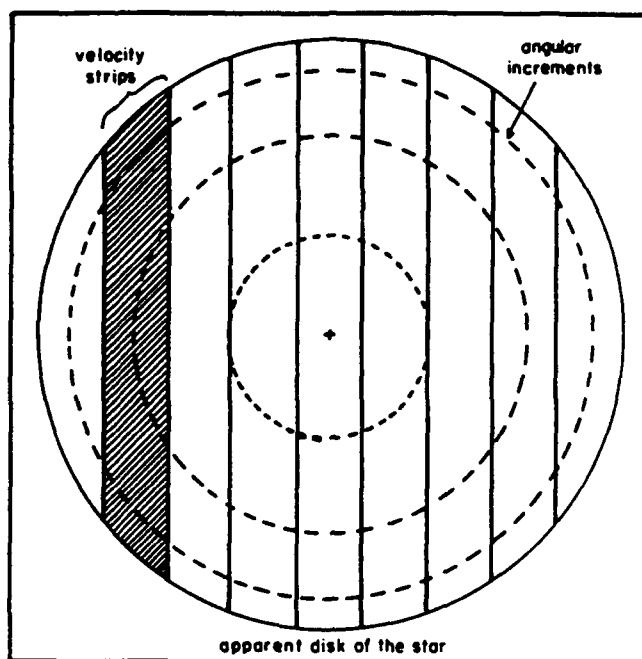


Figure 14: Velocity and angular regions as projected onto the surface of the star. The regions that must be calculated are defined by the intersection of these geometric regions.

Figure 15 shows the results of applying VEL to Ti $\lambda 6258.1 \text{ \AA}$ for three different rotational velocities. These results agree with theory and show that rotation effects can be quite significant. Solar rotation is 2 km/sec, and has little effect on line profiles.

Stellar rotational broadening

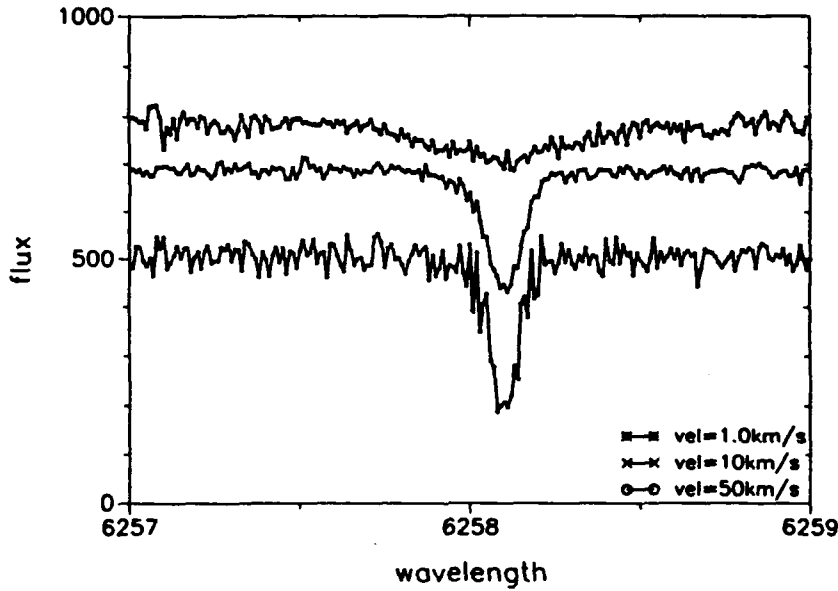


Figure 15: Different rotational velocities as applied to Ti $\lambda 6258.1\text{\AA}$. The top line is for a rotational velocity of 50 km/sec, the middle line is for rotational velocity of 10 km/sec, and the bottom line is for 1.0 km/sec. The flux offset is induced for viewing clarity.

B. COLLISIONAL EXCITATION AND DE-EXCITATION

A major step towards making SAM a fully NLTE simulation is the introduction of collisional processes. Photons need to be added as a result of collisional excitation of an atom followed by photo-de-excitation. In addition, photons need to be removed as a result of photo-excited atoms which undergo collisional de-excitation.

The key to each of these processes is the value of the collisional excitation (C_{lu}) and de-excitation (C_{ul}) rates. From Jefferies [Ref. 16], a semi-empirical equation based on the dipole approximation provides a means to calculate the excitation rate (C_{lu}) from the lower to the upper state.

$$C_{lu} = 2.16\alpha^{-1.68} \exp(-\alpha) T^{-1.5} f n_e \quad (5)$$

where $\alpha = \frac{\eta_o}{KT}$,

η_o = energy of excitation,

n_e = electron density,

f = oscillator strength, and

T = temperature.

With the value of C_{lu} known, calculation of C_{ul} follows from the principle of detailed balance. This principle states that, in TE, all processes occur exactly as rapidly as their inverse. Although TE is required to derive this equation (eq 6), the fact that it only contains various atomic parameters that are properties only of the atoms themselves allows the equation to be valid under NLTE conditions as well. The equation

$$C_{ul} = \frac{g_l}{g_u} \exp\left(-\frac{\eta_o}{KT}\right) C_{lu} \quad (6)$$

where g_l = statistical weight lower level, and

g_u = statistical weight upper level

can be used to relate these two collisional rates.

To compute the number and starting depth of the photons produced by the collisional excitation process, the sum of all the photons produced by this collisional process is first calculated from the starting depth of the blackbody photons (z_0) to the exit altitude of the atmosphere (z_f). The equation for the total number of collisional photons from depth z_0 to z_f is

$$N_{C_{ul}} = \sum_{z_0}^{z_f} C_{ul}(z) \Delta z \quad (7)$$

and for the blackbody photons is

$$N_{bb} = \frac{2\pi c}{\lambda_0^4} \frac{1}{e^{\frac{hc}{KT}} - 1} \quad (8)$$

where: $N_{C_{\mu}}$ = Total number of collisional photon / cm^2 from z_0 to z_f , and

N_{bb} = Number of blackbody photon / cm^2 .

In this way a ratio of the number of blackbody photons to collisionally-produced photons can be found. For example, if the ratio of blackbody photons to collisionally-produced photons is 1 to 3, for every blackbody photon SAM generates, it must also produce three collisionally-produced photons. A collisional photon vs. depth distribution is also calculated during the summing of the collisional photons. Collisionally-produced photons are assigned a starting depth randomly based on this probability distribution.

Photon removal caused by collisional de-excitation is calculated in the line interaction subroutine. If a photon is absorbed by an atom, then a collisional de-excitation probability is checked against a random number and those photons that fall within the de-excitation probability are removed.

In this way, the collisional source function, dependent on depth, and its accompanying extinction process are simulated. Unlike typical treatments by radiative transfer theory, SAM's source function does not need to include photo-excitation and de-excitation. These processes are inherent by the way SAM follows individual photons.

Figures 16 and 17 show the SAM-generated Ti $\lambda 6258.1 \text{ \AA}$ line with and without the collisional source function included. Note the line without the collisional source function (Figure 16) is deeper than the line with the source function included. This effect is caused by an imbalance between photons being produced by collisional excitation and photons being destroyed by collisional de-excitation. In the outer photosphere there are more photons added by collisional excitations than

removed by collisional de-excitation.

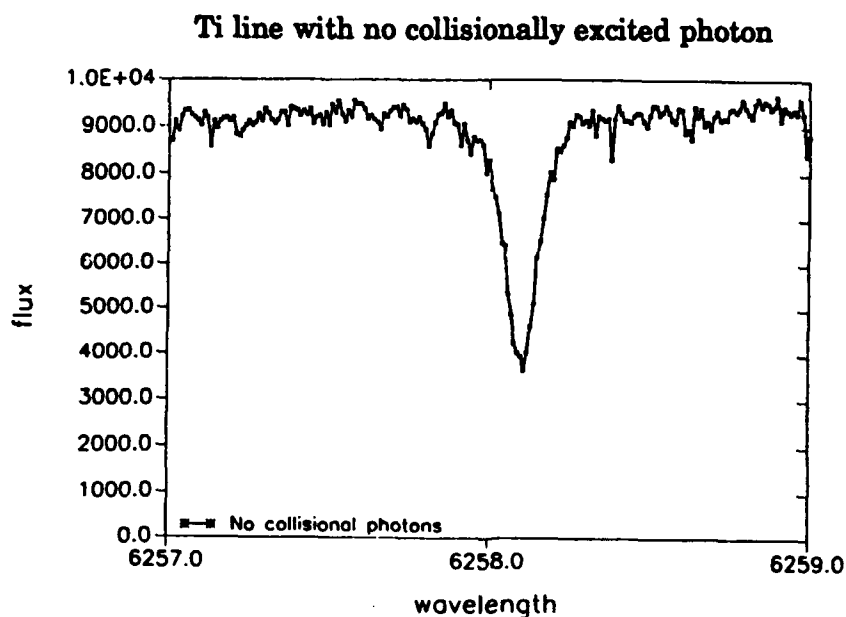


Figure 16: SAM generated line with no collisionally-produced photons added.

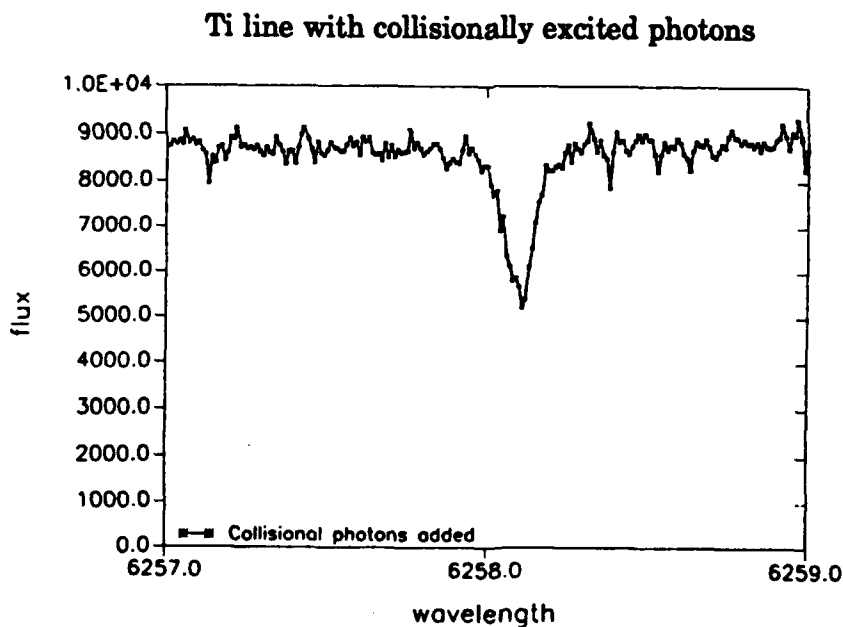


Figure 17: SAM generated line with collisionally-produced photons added.
Note that the line depth has decreased due to the increased number of photon from collisional excitation.

C. INTERPOLATION TABLES

In an effort to reduce the program's computation time, an analysis of SAM's computation properties was undertaken. The results indicated the computer, a Sun SPRAC1 workstation, was spending a significant amount of CPU time calculating and re-calculating atmospheric parameters. Specifically, the subroutine STAR, where spline fits to atmospheric parameters were being calculated, was the largest user of CPU time.

A simple re-design of the subroutine, replacing the spline fits with interpolation tables, was completed. The interpolation tables are calculated in NSUM using the same spline fit routine. The interpolation tables are incremented in 1 km distances. This distance may be varied when stars other than the sun are examined. To ensure no detail in the structure of the atmosphere is lost, graphs of all atmospheric parameter were compared to the interpolation tables (see Appendix A). The net effect of this re-design is a 300% increased in algorithm efficiency with negligible decrease in accuracy.

D. OPTIMIZATION OF PHOTON STARTING DEPTH

Another significant degradation to computation speed is the chosen photon starting depth. It was found that photons which started too deep within the star would undergoes needless absorption and re-emission. A starting depth which minimized computer time is in order. The depth chosen is where the line absorption and continuum absorption processes had identical optical path lengths. Above this point in the atmosphere, the difference between these two optical path lengths shaped the outgoing photon flux. Below this point, the differences in the path length may shape the outgoing flux, but the flux is completely re-ordered as it migrates through the equal path length region. Figure 18 shows $\text{Ti } (\lambda 6258.1 \text{ \AA})$ line generated at the optimal depth (484km) and one generated with z equal to 490km.

There is little different between the two line profiles, but the computer run time for the line profile with z equal to 484km is 10% as fast.

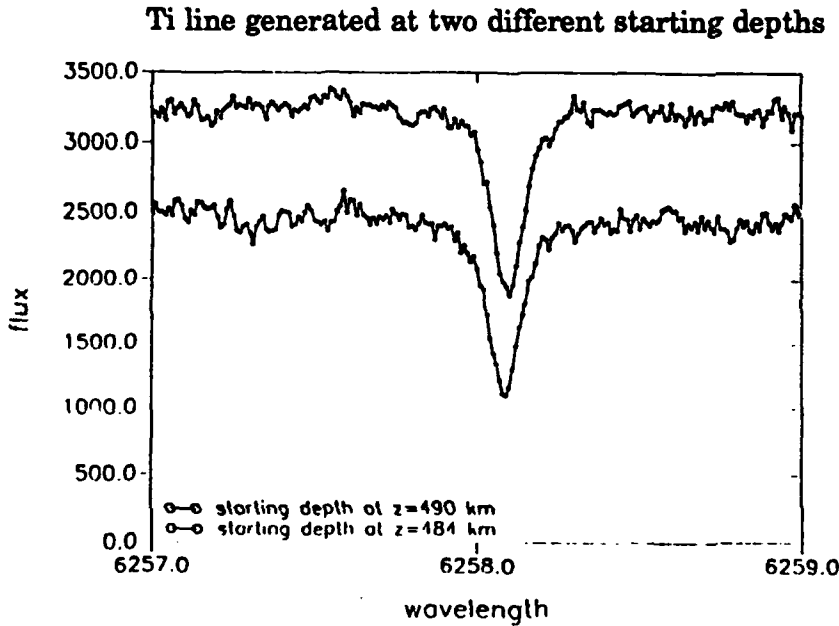


Figure 18: The same Ti line started at two different starting depth. Note that the line shape is almost identical. Difference in flux of the two lines is induced for viewing clarity.

E. REDISTRIBUTION

Photons undergo many different absorption and scattering processes while propagating through the stellar atmosphere. How these photons are redistributed in frequency is of great importance in determining the final line profile. SAM1_13 had two simplified redistribution functions; complete Compton-scattering redistribution for the continuum absorption process, and modified complete Doppler redistribution for the line absorption process. These two simplification are unsuitable for accurate line profile simulation. Improvement to both frequency redistribution functions is necessary.

The major source of continuum absorption in the sun is from H^- . H^- has a low ionization energy at .754 ev, therefore photons with wavelengths less than 16,450 Å have enough energy to ionize H^- . Compared to other sources in the visible region of the continuum, H^- is stronger by a factor of 4 than that due to neutral H and much larger than that for other processes. Therefore, for the sun, all continuum absorption is assumed to be caused by H^- . This assumption is valid for many types of stars. H^- low ionization energy results in a simple redistribution function. All photons absorbed by the continuum process are completely redistributed in frequency. In consideration of minimizing computation efforts, photons redistributed out of the wavelength region of interest are replaced by the introduction of a random wavelength photon from these other regions. In this way, photon flux is conserved.

The line-absorption frequency-redistribution function is a combination of Doppler redistribution (Gaussian in shape) and collisional redistribution (Lorentzian in shape). It is the combination of these two distributions that result in the familiar Voigt profile for line emission and absorption. The rate of collisions, the Voigt α parameter, the kinetic temperature, and the spontaneous emission coefficient (Einstein A), are all important factors in determining line-absorption frequency-redistribution. Doppler redistribution is based on atoms having Maxwellian velocity distribution [Ref. 17]. The standard Gaussian profile is given by

$$P(x) = \frac{e^{-x^2/2\sigma^2}}{\sqrt{2\pi} \sigma}, \quad (9)$$

where: σ = half width at half maximum.

The Doppler redistribution function from Hummer [Ref. 18] is given by

$$\phi(v) = \frac{e^{-v^2/\Delta_d^2}}{\sqrt{\pi} \Delta_d}. \quad (10)$$

If we let $\Delta_d = \sqrt{2}\sigma$, then

$$\phi(v) = \frac{e^{-x^2/2\sigma^2}}{\sqrt{2\pi}\sigma} = P(x) \quad (11)$$

where $\sqrt{2}\sigma = \Delta_d = \frac{\lambda_0}{c} \sqrt{\frac{2KT}{M}}$,

λ_0 = initial wavelength,

c = speed of light,

K = Boltzman constant,

T = kinetic temperature,

M = mass of the atom,

Δ_d = average Doppler shift.

For the collisional redistribution, the standard Lorentzian profile is given by

$$P(x) = \frac{1}{\pi\sigma(1+\frac{x^2}{\sigma^2})} \quad (12)$$

The collisional redistribution function from Hummer [Ref. 18] is given by

$$\phi(v) = \frac{(\Delta^n + \Delta^c)}{\pi((\Delta v)^2 + (\Delta^n + \Delta^c)^2)} \quad (13)$$

where Δ^n = average natural broadening,

Δ^c = average collisional broadening.

Let $\sigma = \Delta^n + \Delta^c$ and rearranging

$$\phi(v) = \frac{1}{\pi\sigma(1+\frac{x^2}{\sigma^2})} = P(x). \quad (14)$$

The Voigt a parameter is

$$a = \frac{\Delta^n + \Delta^c}{\Delta_d} ,$$

therefore $\sigma = \Delta_d a$.

Normal random number distribution was modified by the Box-Muller method [Ref. 19] to produce a temperature-dependent Gaussian (eq 15). Random Lorentzian distribution dependent on the Voigt α parameter and temperature was produced by inverse transform method (eq 16)[Ref. 19].

$$\lambda \text{ shift} = \sqrt{-2\ln(r)} \cos(2\pi r) \sqrt{\frac{KT}{M} \frac{\lambda_0}{c}} \quad (15)$$

$$\lambda \text{ shift} = \tan(\pi r) \sqrt{\frac{2KT}{M} \frac{\lambda_0}{c} a} \quad (16)$$

where r = random number between zero and one.

These redistribution functions were tested by generating a million random numbers and plotting the resulting $\lambda \text{ shift}$ (Figure 19 and 20).

Gaussian redistribution function

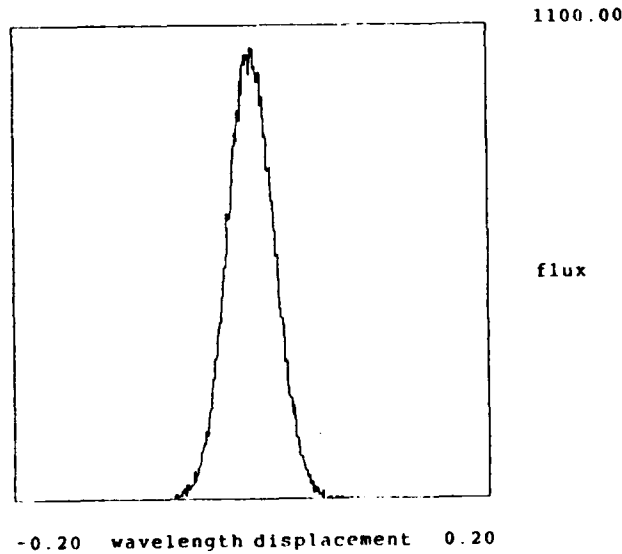


Figure 19: Gaussian curve produced by redistribution function.

Lorentzian redistribution function

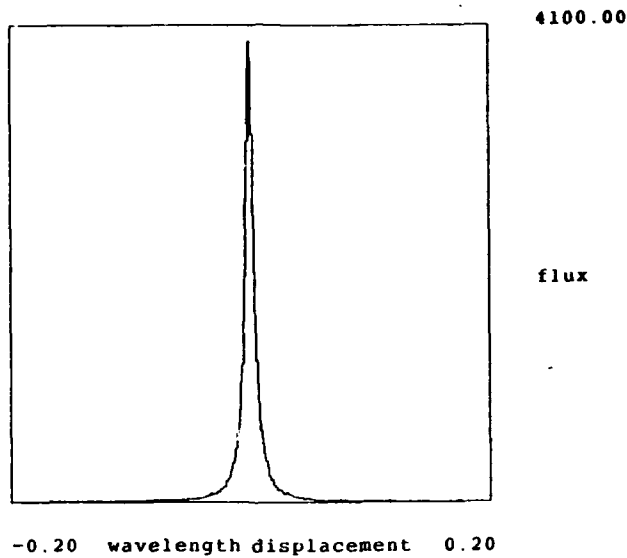


Figure 20: Lorentzian curve produced by redistribution function.

Since collisional redistribution is dependent on whether an atom undergoes a collisional interaction, not all line-absorbed photons are collisionally redistributed. As a first order approximation, it can be assumed that the ratio of collisional de-excitation compared to total de-excitation is the same as the ratio of photons which undergoing collisional redistribution compared to just Doppler redistribution.

It is with these two redistribution functions (eq 15 and 16) that re-emitted photons are redistributed in wavelength in SAM. The photons, once absorbed, are re-emitted with a new wavelength assigned randomly by a combination of these two functions. These functions are a major improvement over the simplified functions being used in SAM1_13.

IV. TESTING AND RESULTS

Three methods of testing the validity of SAM were undertaken. The first method involved comparisons of theoretical mean free path lengths to computed mean free path lengths in a homogeneous atmosphere. The second method is comparison of observed absorption line profiles to SAM-generated profiles. Finally, observational limb darkening is compared to SAM-generated limb darkening. To demonstrate the flexibility of SAM, stellar turbulence and stellar wind effects are applied to the solar Ti $\lambda 6258.1 \text{ \AA}$ line.

A. MEAN FREE PATH

In this test both the line absorption subroutine and the continuum absorption subroutines are tested. Although stellar atmospheres are not homogeneous, the homogeneous assumption allows mean free path calculations to be made. Therefore this is an important test for SAM. Mean free path calculations are shown below.

Treating the atmosphere as homogeneous and including only absorption processes of the continuum, the expected normal exponential decay equation is obtained.

$$\frac{I}{I_0} = \exp(-\kappa_v \rho L) \quad (17)$$

where: I = intensity at distance L through the medium

I_0 = initial intensity,

κ_v = continuum opacity per gram, and

ρ = density.

The average length (L_{ave}) is;

$$L_{ave} = \frac{1}{\kappa_v \rho} \quad (18)$$

where κ_v and ρ are given by the photospheric model being used.

For the mean free path of the line absorption process, the equation is;

$$\frac{I}{I_0} = \exp(-\kappa_{v_i} L) . \quad (19)$$

Therefore,

$$L_{ave} = \frac{1}{\kappa_{v_i}} \quad (20)$$

where

$$\kappa_{v_i} = \frac{\sqrt{\pi} e^2}{mc} \frac{g_u f N_i 10^{-\theta \chi}}{\Delta v_D U} H(u, a) ,$$

f = oscillator strength,

g_u = statistical weight upper level,

U = partition function of the atom,

N_i = population level of i state,

$\theta = 5039.99/\text{kinetic temperature}$,

χ = excitation energy of lower level (eV),

Δv_D = Doppler shift, and

$H(u, a) = \text{Hjerting function}$.

SAM generated L_{ave} values were produced by averaging 3000 path lengths through the homogeneous medium. Table 1 and 2 contains various input parameters as well as both calculated L_{ave} and SAM-generated L_{ave} . Mean free path comparisons for the continuum subroutine are done for four different continuum optical depths, while the line absorption subroutine are done for four different line optical depths.

TABLE 1 :CONTINUUM					
τ	depth (km)	$\kappa_v(\frac{cm^2}{g})$	$\rho(\frac{g}{cm^3})$	$L_{ave}(km)$ [theory]	$L_{ave}(km)$ [SAM]
.001	83	1.28×10^{-2}	1.37×10^{-8}	56800	56300
.01	213	3.61×10^{-2}	4.88×10^{-8}	5670	5630
.1	344	1.10×10^{-1}	1.59×10^{-7}	569	565
1.0	455	.945	3.31×10^{-7}	31.9	33.9
10.0	500	17.5	3.15×10^{-7}	1.81	1.90

TABLE 2 :LINE					
τ_i	depth (km)	H(u,a)	$\kappa_v(cm^{-1})$	$L_{ave}(km)$ [theory]	$L_{ave}(km)$ [SAM]
.05	55	.9628	9.09×10^{-9}	1100	1109
.18	83	.9497	2.14×10^{-8}	467	463
3.17	213	.8569	1.49×10^{-7}	67.2	66.0
15.0	344	.6079	4.35×10^{-7}	22.9	22.9

A comparison of the results reveals the good agreement between the typical mean free paths calculated by SAM and those predicted by theory. The minor difference between the two values may be accounted for by the averaging of the random processes.

B. COMPARISON TO OBSERVATION

The second method of validation is the comparison of the computer generated lines to observed lines. Line observations are taken from the National Solar Observatory Atlas [Ref. 20].

1. Convergence

Figures 21, 22 and 23 show a time series from SAM. Since SAM is a Monte Carlo simulation, the more photons SAM generates, the higher the resulting signal to noise ratio in the SAM generated curve becomes. The trade off can be seen in these three figures. All SAM line profiles were generated on a Sun SPRAC1 workstation and CPU times stated are from this computer. Figure 21 required only 2 minutes of CPU time and produced 10,000 photons. Figure 22 required 20 minutes of CPU time and produced 100,000 photons. Figure 23 required about 200 minutes of CPU time producing 1,000,000 photons.

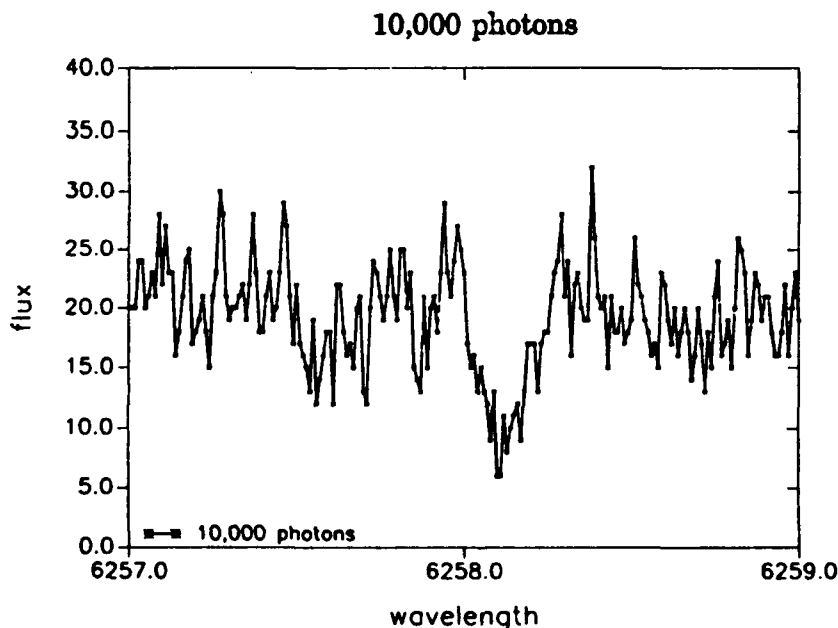


Figure 21: 10,000 photons produced by SAM in 2 minutes

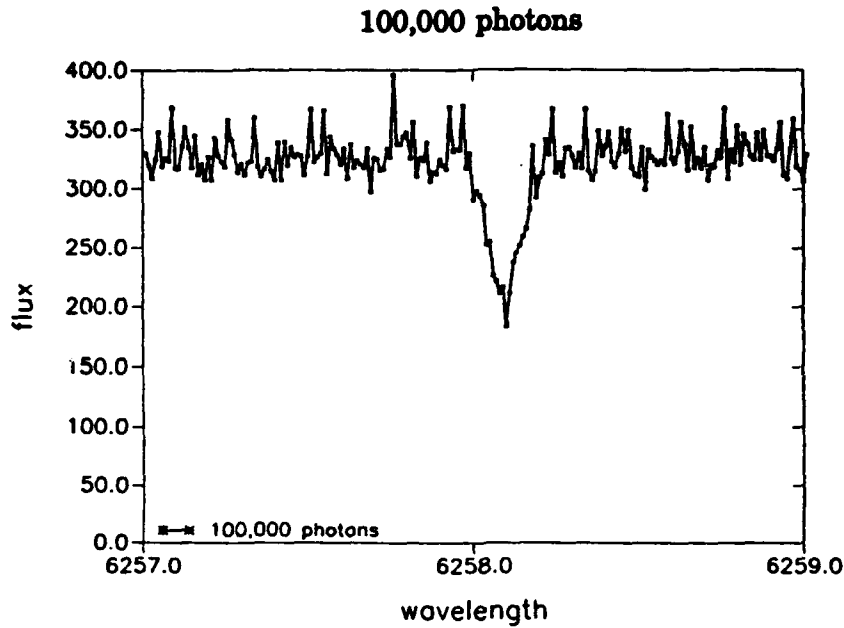


Figure 22: 100,000 photons produced by SAM in 20 minutes.

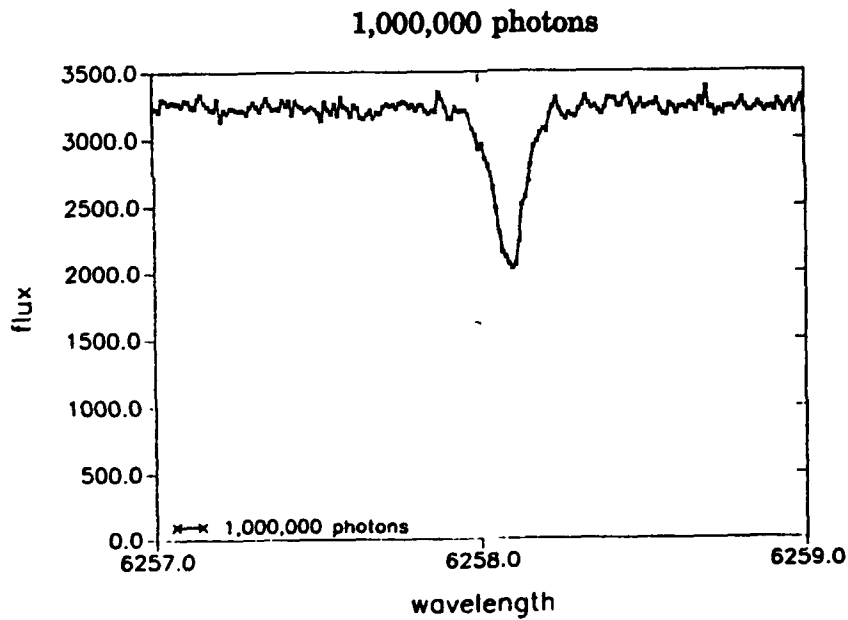


Figure 23: 1,000,000 photons produced by SAM in approximately 200 minutes.

Standard fluctuation calculation reveals that the fluctuation per bin is in agreement with random processes.

$$F = \sqrt{N_{ave}} \quad (20)$$

where: F = Fluctuation per bin, and

N_{ave} = Average number of photons per bin.

2. Line synthesis

One of the major applications of SAM is the fitting of stellar and atomic parameters. For this thesis, three solar line are synthesized. The portions of the solar spectrum being synthesized are shown in Figures 24, 25 and 26. The figures show two sets of lines. The dark line is the intensity of the solar flux on a scale between 0 and 100%. The lighter line is the more detailed scale running from 90 to 100%. It is the darker line that SAM is modeling. The wavelengths given in these figures are in nanometers. These lines were chosen principally because of the availability of the two atomic constants; spontaneous emission coefficient (Einstein A), and quadratic stark interaction constant (C_4). For comparison to SAM generated lines, the absorption lines near the absorption line being modeled have been replaced by a smoothed continuum.

Observed portions of solar spectrum

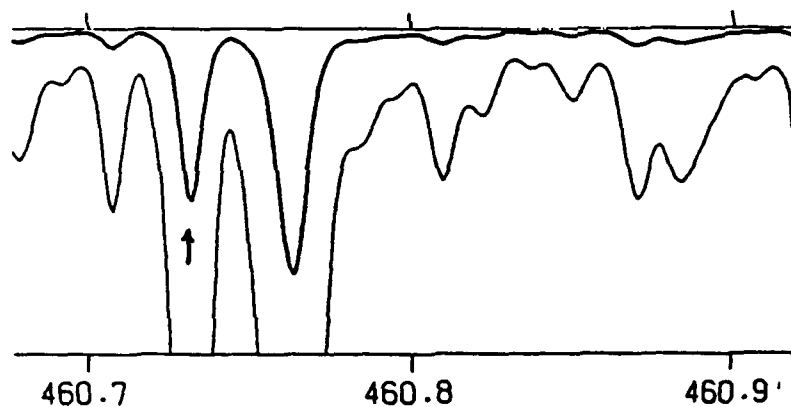


Figure 24: Observed solar spectrum near $\text{Sr } \lambda 4607.3$ absorption line.

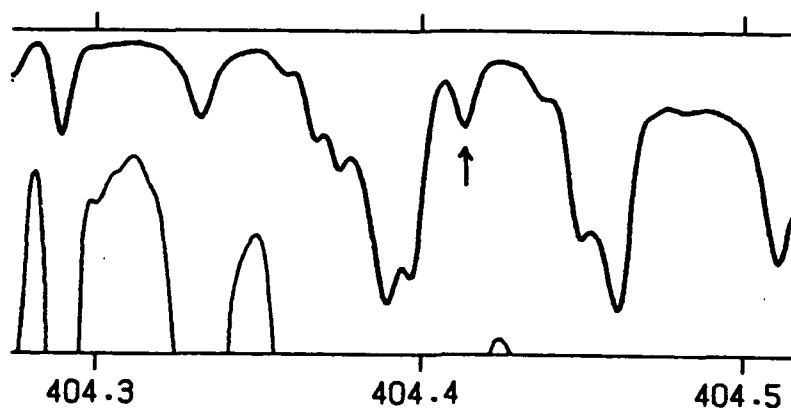


Figure 25: Observed solar spectrum near K $\lambda 4044.1$ absorption line.

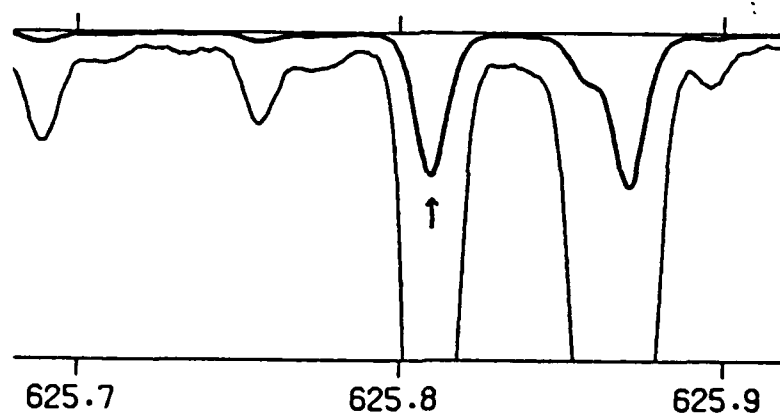


Figure 26: Observed solar spectrum near Ti $\lambda 6258.1$ absorption line.

Initial comparisons to estimated abundance, and C4 values are shown in Figures 27, 28, and 29. Notice that most of the fits lack the required line strength and line broadening. Abundance values are given as the log of the ratio of atom abundance to hydrogen abundance, with $\log H$ abundance = 12.0.

Comparison of observed lines to SAM-generated lines
using initial C4 and abundance values

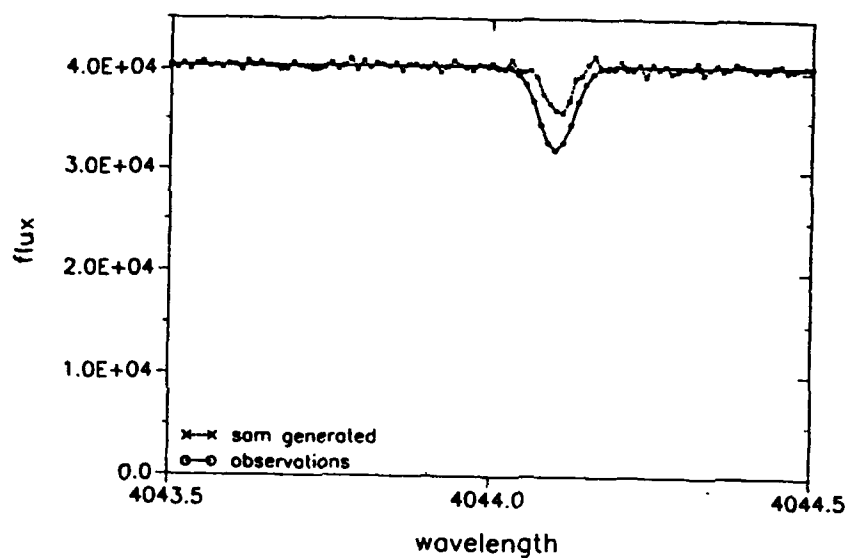


Figure 27: Observed K λ 4044.1 line to SAM-generated line with abundance = 5.6 and log C4 = -13.59.

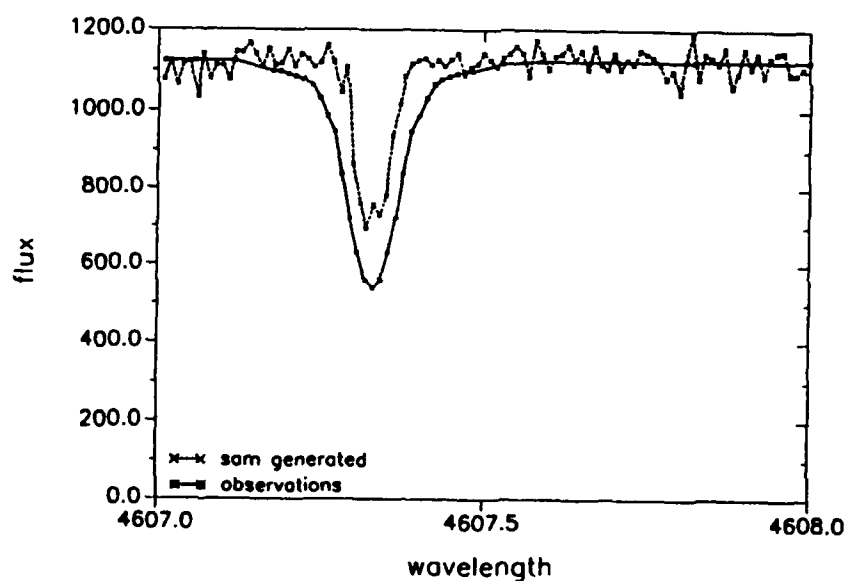


Figure 28: Observed Sr λ 4607.3 line to SAM-generated line with abundance = 2.7 and log C4 = -15.81.

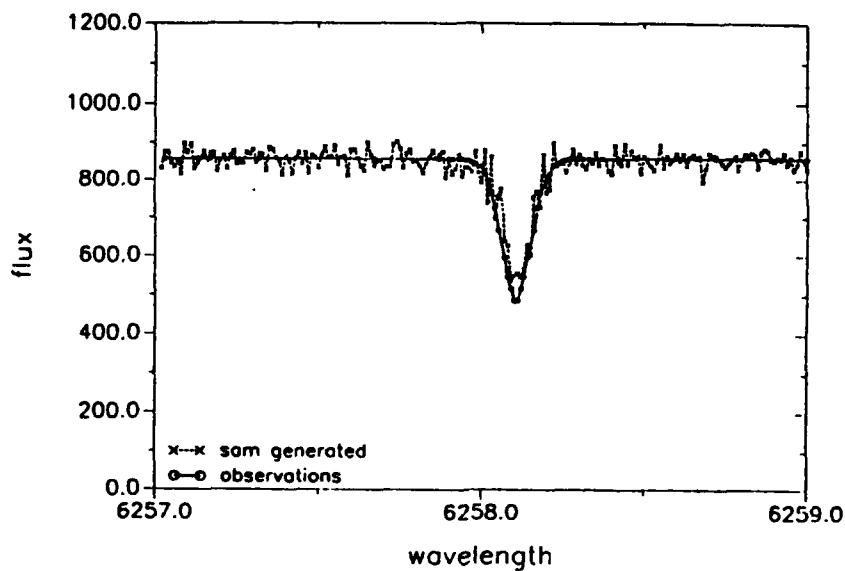


Figure 29: Observed Ti λ 6258.1 line to SAM-generated line with abundance = 4.78 and $\log C4 = -10.41$.

The initial values of abundance and C4 are adjusted until a good fit is obtained. Adjustment is appropriate as these values typically have a large uncertainty. Figures 30, 31, and 32 show SAM-generated fits with adjusted atomic values. Quality of the fits can be compared to that in Figure 3.

Comparison of observed lines to SAM-generated lines
using adjusted C4 and abundance values

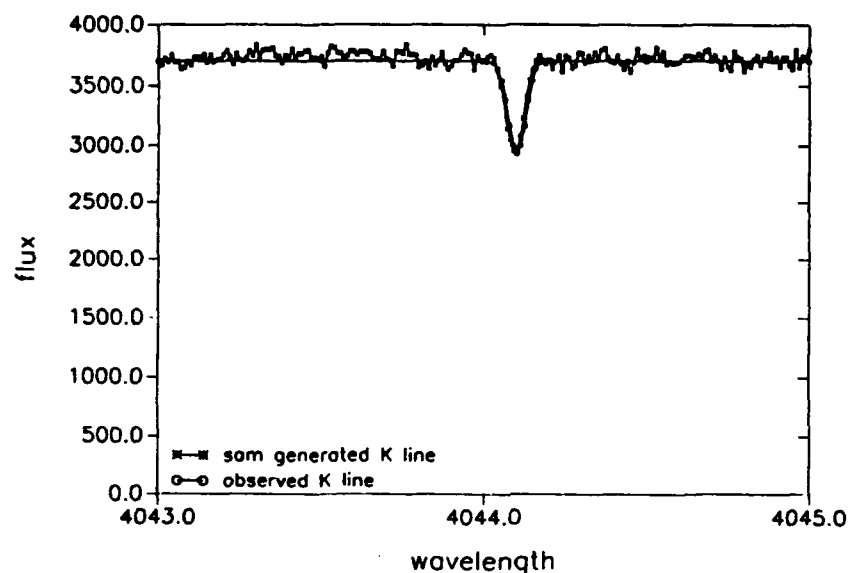


Figure 30: Observed K λ 4044.1 line to SAM-generated line with abundance = 5.81 and log C4 = -11.19.

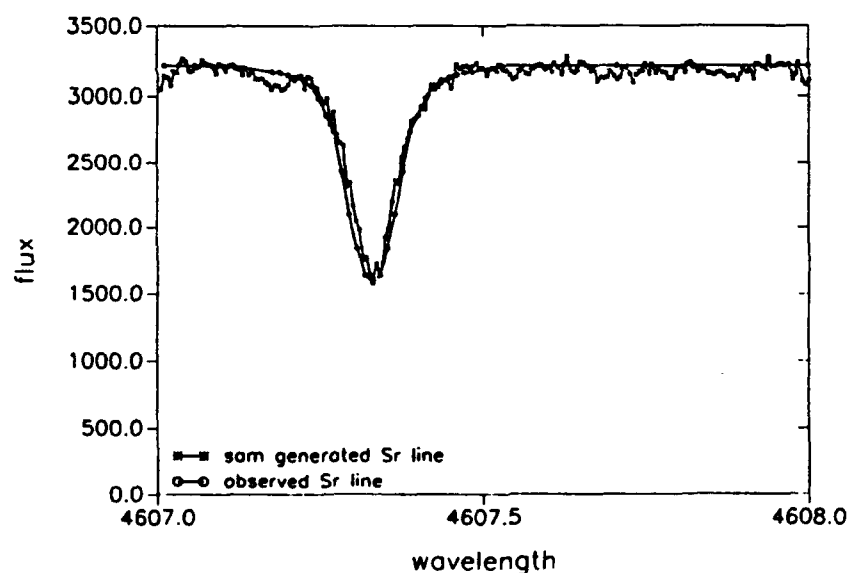


Figure 31: Observed Sr λ 4607.3 line to SAM-generated line with abundance = 3.00 and log C4 = -9.81.

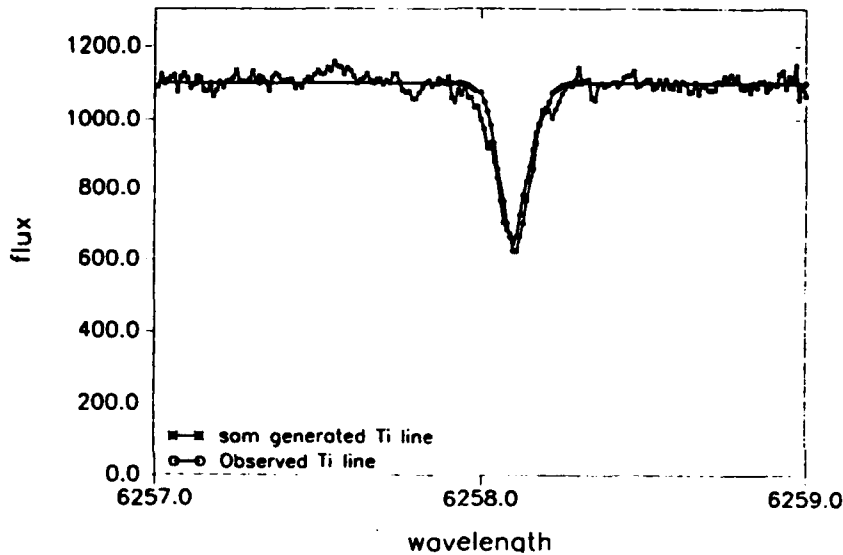


Figure 32: Observed Ti $\lambda 6258.1$ line to SAM-generated line with abundance = 4.80 and $\log C4 = -10.41$.

C. LIMB DARKENING

Solar radiation intensity (ergs/cm^2) decreases from the center of the solar disk to the limb. This limb darkening effect is caused by successive viewing of higher and higher photospheric layers, where temperature is lower and the source function is less intense. It is the limb darkening effect that allows temperature distributions and approximate source functions to be determined as a function of height in the stellar atmosphere. These are important parameters for stellar modeling. The understanding and successful simulation of this effect is therefore applicable and relevant.

The SAM simulation retains two pieces of information on exiting photons: photon wavelength and exit angle from the surface normal. If SAM's output is considered spread uniformly over the solar disk then the angular binning of the exiting photons gives the exit location of the photons. But limb darkening measurements are taken from a thin spatial region from the center of the solar disk to its edge. These measurements in effect reduce the sun's intensity into a 2

dimensional cross section, where the intensity is a function of angular position. But observations of limb darkening are made in terms of intensity (*photons/cm²*), therefore each angular region's exiting photon flux must be divided by the projected surface area normal to the observer to obtain the necessary intensity. Figure 33 shows a comparison of SAM-generated limb darkening for 5000Å to observed curve. Agreement is good until the SAM-generated limb intensity becomes greater than observations around 70 degrees.

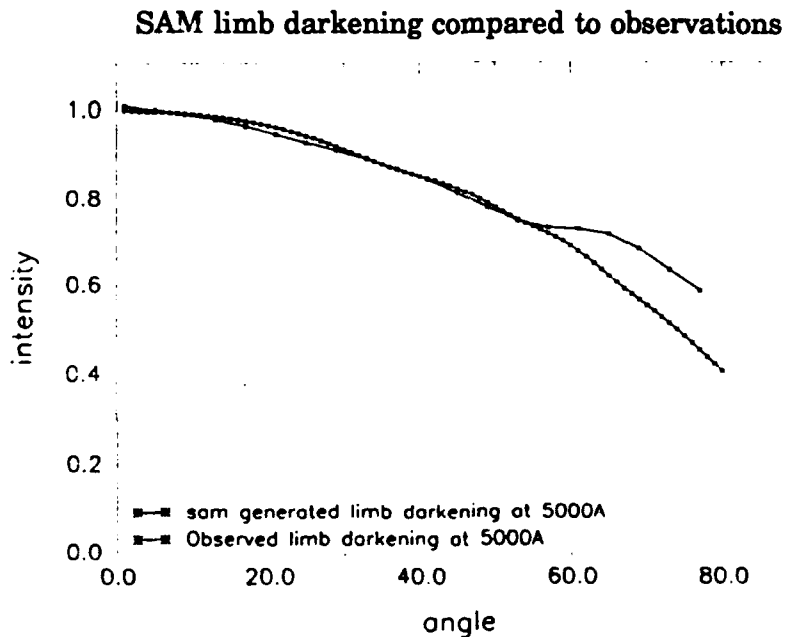


Figure 33: SAM generated limb darkening at 5000Å compared to 5000Å observed curve. Deviation is still under investigation.

Investigations into this effect seem to indicate it is related to the continuum opacity κ_v but earlier mean free path calculations indicate κ_v is calculated correctly.

D. STELLAR TURBULENCE

Turbulence is the motion of the atmospheric gases on a scale that is large compared to atomic dimensions but small compared to the size of the star. Eddies, convection cells, and prominence-like structures are all forms of turbulence. These motions cause additional Doppler shifting to the photons and can greatly affect the line shape.

The velocity Doppler shifting due to stellar turbulence occurs in SAM during the calculation of the line-absorption coefficient. SAM does not currently Doppler shift the photons due to stellar turbulence during re-emission. This would be fairly easy to correct if the nature of the turbulence is known. For the purpose of this thesis the re-emission correction is ignored. The broadening caused by increasing the stellar turbulence velocity to the Sr $\lambda 4607.3 \text{ \AA}$ is shown in Figure 35.

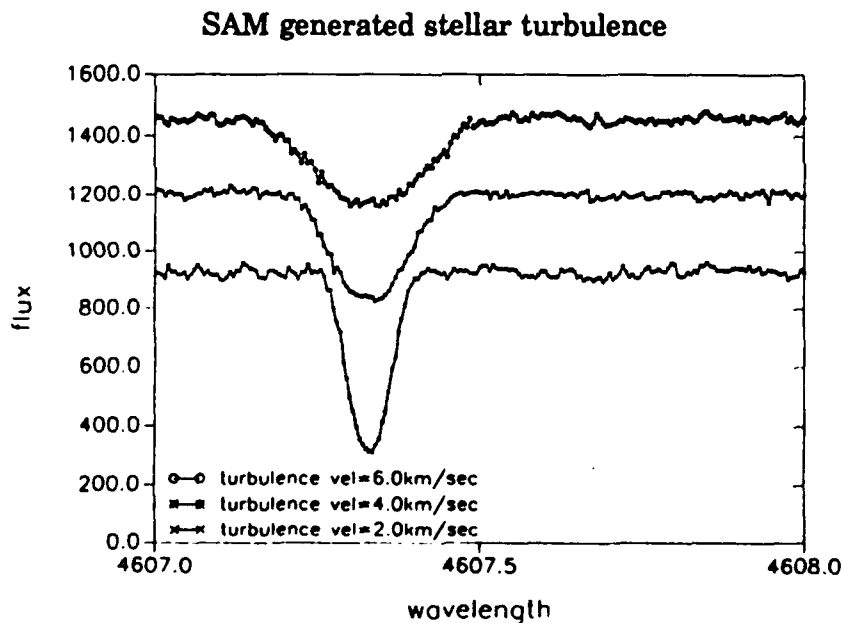


Figure 35: SAM generated stellar turbulence for three different velocities. The top line is for a turbulence velocity of 6.0 km/sec, the middle line is for 4.0 km/sec, and the bottom line is for 2.0 km/sec. Offsets are induced for viewing clarity.

E. STELLAR WINDS

Stellar winds differ from turbulence in that the gases driven by convection or radiation obtain the necessary velocity to escape from the star. The amount of escaping matter can be quite large, typically 1 earth mass per year. The effects of this escaping matter on stellar lines is not well known. Although some general aspects of stellar wind effects on line profiles can be anticipated. The rapidly moving matter will most certainly Doppler shift emitted photons. The Doppler shifting will only be in blue direction as the material which is moving away from the observer will be blocked by the star. Consequently, line profiles should contain increased flux in the shorter wavelengths. Many additional effects and the driving forces of these winds are not well known. This is one of the motivations behind the creation of SAM.

In an effort to test the stellar wind routine in SAM, a 10 km/sec maximum stellar wind was imposed on the sun. Although this is clearly unrealistic, the goal was to reproduce some of the effects of stellar winds on a known spectrum. The wind speed varied linearly with altitude, reaching a maximum of 10 km/sec at the top of the photosphere. the equation for this variation is

$$\text{wind velocity} = \frac{z}{z_{\text{max}}} \text{maximum wind velocity} , \quad (22)$$

where z = distance out of the photosphere from reference depth (500km),

z_{max} = distance to top of photosphere from reference depth.

Figure 36 shows the effect of this wind on the earlier synthesized Ti absorption line. The large emission spike at the shorter wavelengths is the same effect observed in stars with large stellar winds [Ref. 21]. This is an exciting initial result. To emphasize the ease in which SAM was modified, only four additional lines of code were required to simulate movement of the outer photosphere. Two additional wind velocities were also run as shown in Figures 37 and 38.

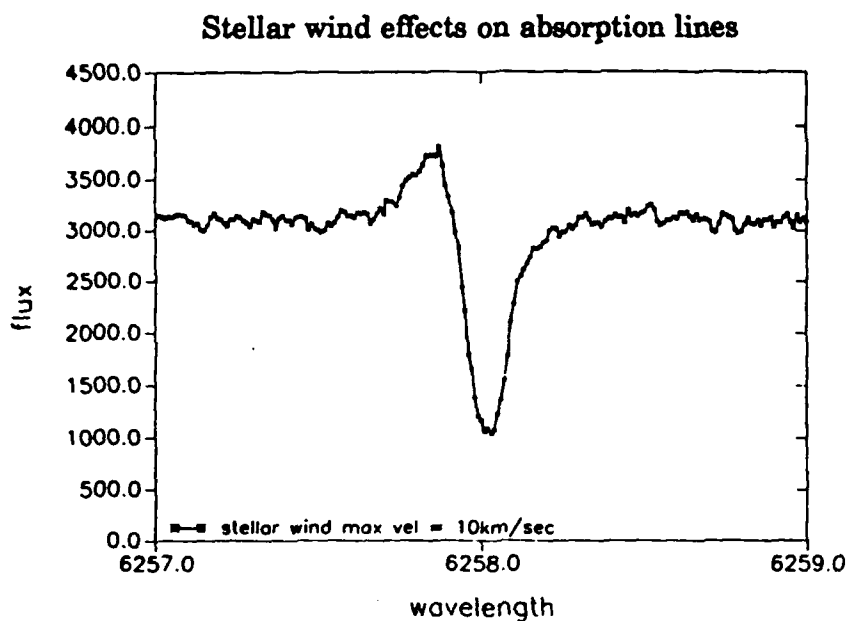


Figure 36: SAM generated absorption line with 10 km/sec maximum stellar wind.

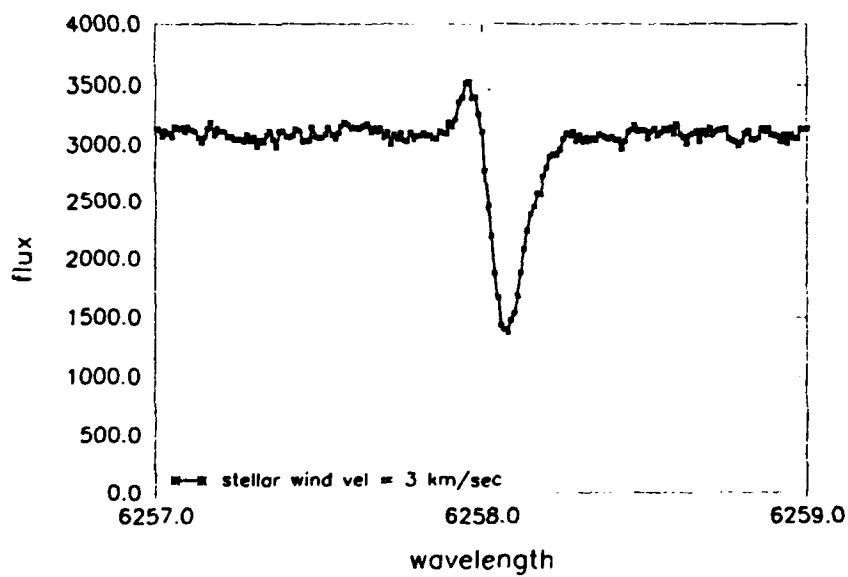


Figure 37: SAM generated absorption line with 3 km/sec maximum stellar wind.

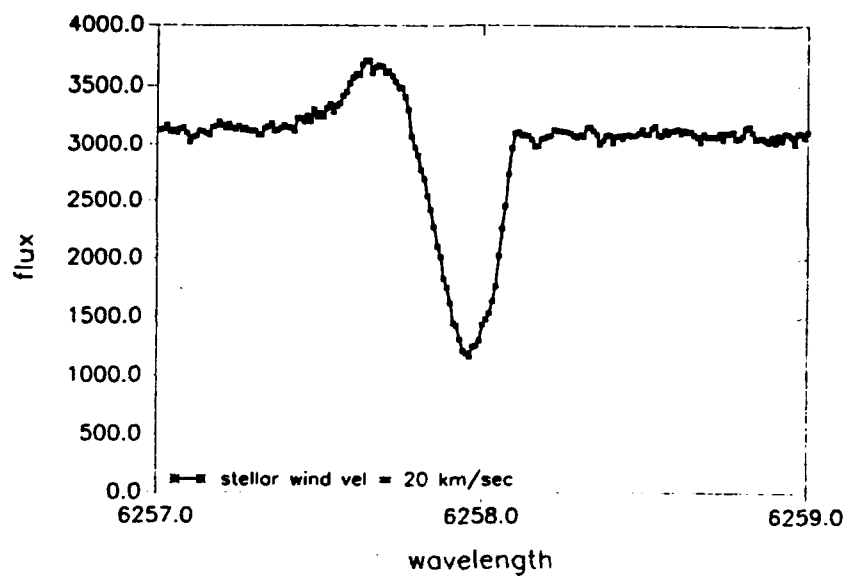


Figure 38: SAM generated absorption line with 20 km/sec maximum stellar wind.

V. CONCLUSION

The primary goal of this thesis has been the modification and testing of a new photon-following approach to stellar radiative transfer. The approach has several major advantages over standard stellar radiative transfer methods and has only recently been possible with the aid of fast computers. It was demonstrated that this technique accurately and efficiently reproduced observed solar absorption lines, including the effects of stellar rotation, stellar turbulence, collisional excitation, and collisional de-excitation. Stellar winds and limb darkening were reproduced although problems still remain in these areas. Nevertheless, the successful simulation of these effects is an improvement over previous methods. One of the major advantages of this approach to stellar radiative transfer is many vastly-different stellar phenomena can be modeled and incorporated into a single simulation.

To demonstrate the usefulness of this technique, new abundance and C4 values for three solar lines were determined. This technique can also be used to investigate almost all phenomena related to stellar atmospheres and radiative transfer (i.e., testing various model atmospheres, stellar wind theories, stellar turbulence, etc.)

The results described in this thesis used fairly well-behaved stellar absorption lines. An extension of this thesis would be to generate true NLTE atomic population levels in the outer photosphere. If this were accomplished, the complex NLTE lines could be simulated. Some additional extension areas are: accurate representation of the Hjerting function when the Voigt α parameter exceeds unity, new redistribution functions that separate natural and collisional broadening, and improved velocity profiles for both stellar turbulence and stellar winds. Although these problems are non-trivial, there are no foreseeable road blocks for this new technique to simulate a large variety of complex stellar lines.

APPENDIX A. SOLAR ATMOSPHERIC PARAMETERS

In chapter III section C spline fits to atmospheric parameters [Ref. 22] were replaced with interpolation tables. Figures 39 through 42 show a comparison between spline fit curves and interpolation values for temperature, density, opacity and gas pressure as each vary with depth. Incremental distance of 5km was chosen to allow the difference between the two curves to be seen. Better agreement is actually found in SAM because of the use of 1km increments. Note an exception to the 5km increments is Figure 41 where an incremental distance of 2km is chosen because of the reduced distances being plotted.

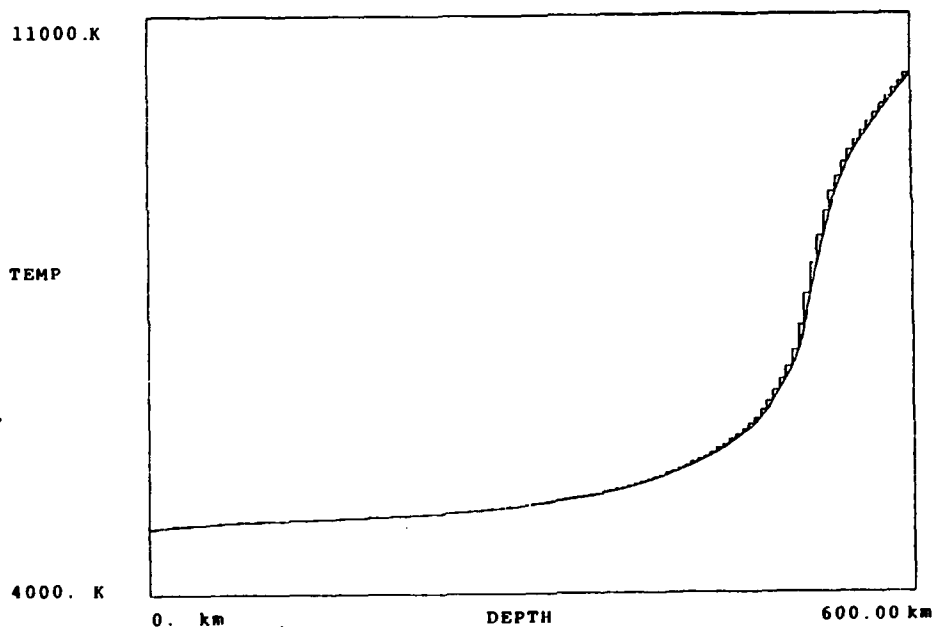


Figure 39: Temperature curve generated by spline fit compare to interpolation tables

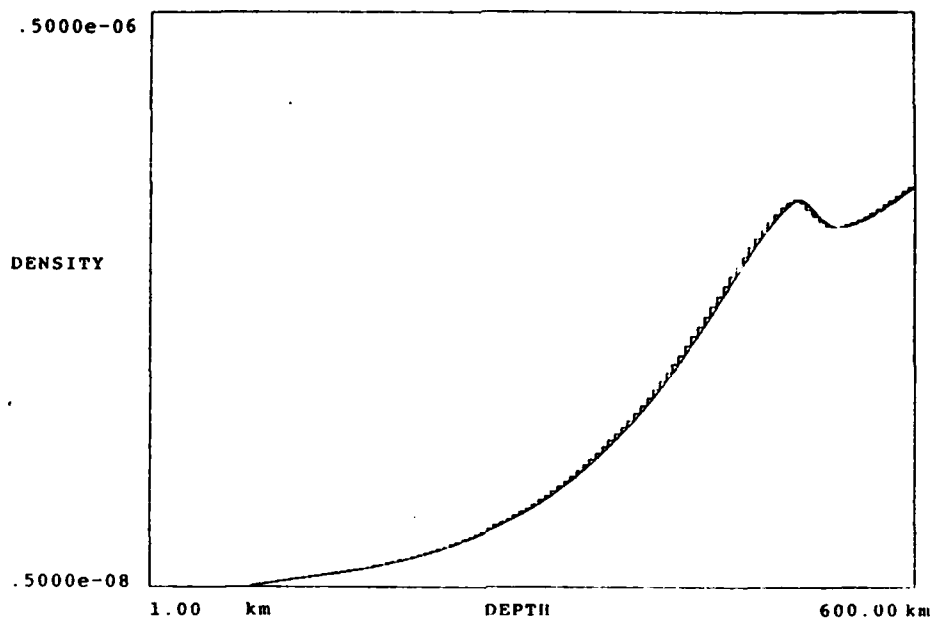


Figure 40: Density ($\frac{g}{cm^3}$) curve generated by spline fit compare to interpolation tables

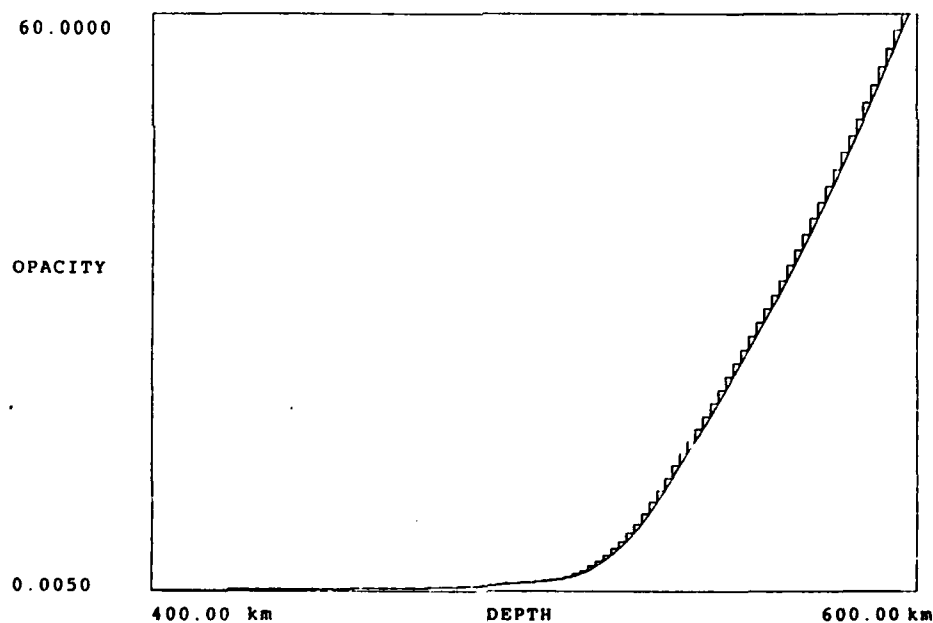


Figure 41: Opacity ($\frac{cm^2}{g}$) curve generated by spline fit compare to interpolation tables

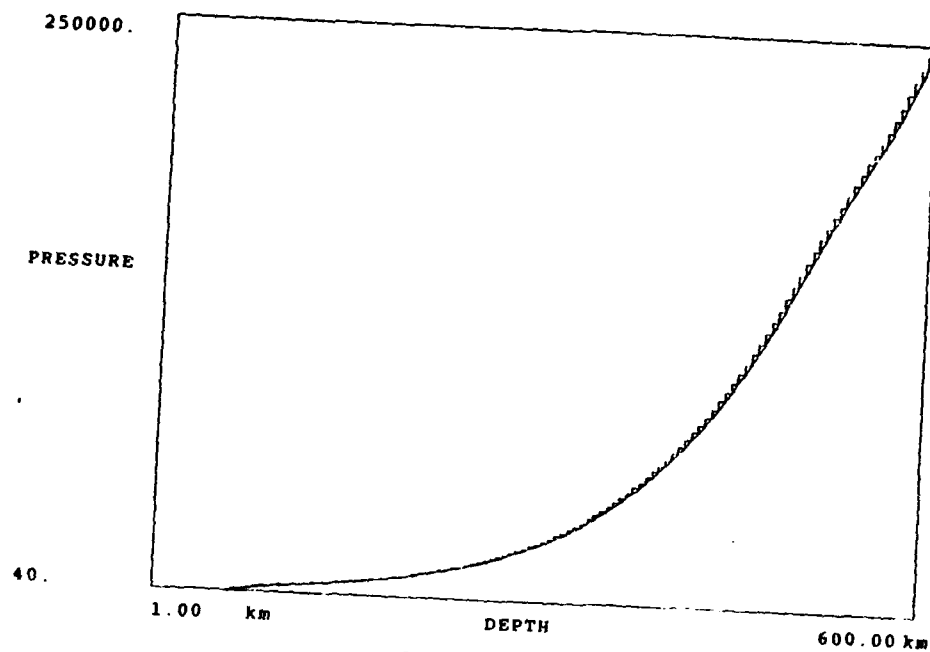


Figure 42: Gas pressure ($\frac{\text{dyne}}{\text{cm}^2}$) curve generated by spline fit compare to interpolation tables

LIST OF REFERENCES

1. Kudritzki, R. P., *The Atmospheres of hot stars: Modern Theory and Observation*, paper presented at the 18th Advanced course of the Swiss Society of Astronomy and Astrophysics, Leysin, Switzerland, March 1988, p 6.
2. Melboure, W. G., *Astrophysical Journal*, vol 132, p 101, 1960.
3. Carbon, D. F. and Gingerich, O., **Theory and Observation of Normal Stellar atmospheres**, MIT Press, 1969, p 377.
4. Curtis, G. W. and Jefferies, J. T., *Astrophysical Journal*, vol 150, p 1061, 1967.
5. Gray, D. F., **The Observation and Analysis of Stellar Photospheres**, John Wiley & Sons, Inc. 1976, p 330.
6. Ross, J. and Aller, L., *Astrophysical Journal*, vol 153, p 235, 1968.
7. Gray, D. F., **The Observation and Analysis of Stellar Photospheres**, John Wiley & Sons, Inc. 1976, p 351.
8. Kudritzki, R. P., *The Atmospheres of hot stars: Modern Theory and Observation*, paper presented at the 18th Advanced course of the Swiss Society of Astronomy and Astrophysics, Leysin, Switzerland, March 1988.
9. Auer, L. H. and Mihalas, D., *Astrophysical Journal Supplement*, vol 24, p 193, 1972.
10. Becker, S. and Butler, K., *Astronomy Astrophysical Supplement*, 1988a.
11. Becker, S. and Butler, K., *Astronomy Astrophysical Supplement*, 1988b.
12. Kudritzki, R. P., *The Atmospheres of hot stars: Modern Theory and Observation*, paper presented at the 18th Advanced course of the Swiss Society of Astronomy and Astrophysics, Leysin, Switzerland, March 1988, p 40.
13. Herrero, A., *Astronomy Astrophysical*, 1987, vol 171, p 189.

14. Abbott, D. C., and Lucy, L. B., *Astrophysical Journal*, vol 288, p 679, 1985.
15. Kudritzki, R. P., Simon, K. P., and Hamann, W. R., *Astronomy and Astrophysics*, vol 118, p 245, 1983.
16. Jefferies, J. T., **Spectral Line Formation**, Blaisdell Publishing Co., 1968, p 118.
17. Mahalas, D., **Stellar Atmospheres**, W. H. Freeman and Co., 1978, p 121.
18. Hummer, D. G., **An Introduction to the Art and Science of Radiative Transfer**, paper presented at Naval Postgraduate School radiative transfer lectures, Monterey, California, May 1990.
19. Gould, H. and Tobehnik, J., **An Introduction to Computer Simulation Methods Applications to Physical Systems Part 2**, Addison-Wesley Publishing Co., 1988, p 340.
20. National Solar Observatory, **Atlas No. 1, Solar Flux from 296nm to 1300nm**, Office of University Publisher, Harvard University, June 1984.
21. National Aeronautics and Space Administration, **Nattional Aeronautics and Space Administration Scientific and Technical Information Division, O Stars and Wolf-Rayet Stars**, Government Printing Office, Washington, DC, 1988.
22. Gingerich, O., **Theory and Observation of Normal Stellar Atmospheres**, MIT Press, 1969, p 367.

INITIAL DISTRIBUTION LIST

- | | | |
|----|--|---|
| 1. | Defense Technical Information Center | 2 |
| | Cameron Station | |
| | Alexandria, Virginia 22304-6145 | |
| 2. | Library, Code 52 | 2 |
| | Naval Postgraduate School | |
| | Monterey, California 93943-5002 | |
| 3. | Wm. Bruce Weaver | 3 |
| | 900 Major Sherman Lane | |
| | Monterey Institute for Research in Astronomy | |
| | Monterey, California 93940 | |
| 4. | Professor David D. Cleary Code PH/CL | 1 |
| | Department of Physics | |
| | Naval Postgraduate School | |
| | Monterey, California 93943-5000 | |
| 5. | Professor K. E. Woehler Code PH/WH | 1 |
| | Chairman, Department of Physics | |
| | Naval Postgraduate School | |
| | Monterey, California 93943-5000 | |